Brown University
DIVISION OF ENGINEERING
PROVIDENCE, R.I. 02912

(2)

MEASUREMENT OF THE TEMPERATURE PROFILE DURING SHEAR BAND FORMATION IN STEELS DEFORMING AT HIGH STRAIN RATES

by

K. A. Hartley, J. Duffy and R. H. Hawley
Division of Engineering, Brown University
Providence, R.I. 02912

2

MEASUREMENT OF THE TEMPERATURE PROFILE DURING SHEAR BAND FORMATION IN STEELS DEFORMING AT HIGH STRAIN RATES

by

K. A. Hartley, J. Duffy and R. H. Hawley
Division of Engineering, Brown University
Providence, R.I. 02912

Army Research Office Report
No. DAAG 29-85-K-0003/2

Materials Research Laboratory
Brown University

March, 1986

UNCLASSIFIED

SECURITY CLASSIFICATION OF THIS PAGE (When Data Entered)

MASTER COPY - FOR REPRODUCTION PURPOSES

REPORT DOCUMENTATION PAGE

READ INSTRUCTIONS BEFORE COMPLETING FORM

1. REPORT NUMBER: ARO 22306.4-EG	2. GOVT ACCESSION NO.: N/A
3. RECIPIENT'S CATALOG NUMBER: N/A	
4. TITLE (and Subtitle): Measurement of the Temperature Profile During Shear Band Formation in Steels Deforming at High Strain Rates.	5. TYPE OF REPORT & PERIOD COVERED: Technical
	6. PERFORMING ORG. REPORT NUMBER:
7. AUTHOR(s): K.A. Hartley, J. Duffy and R.H. Hawley	8. CONTRACT OR GRANT NUMBER(s): DAAG-29-85-K-0003
9. PERFORMING ORGANIZATION NAME AND ADDRESS: Division of Engineering, Brown University, Providence, RI 02912	10. PROGRAM ELEMENT, PROJECT, TASK AREA & WORK UNIT NUMBERS: N/A
11. CONTROLLING OFFICE NAME AND ADDRESS: U. S. Army Research Office, Post Office Box 12211, Research Triangle Park, NC 27709	12. REPORT DATE: March, 1986
	13. NUMBER OF PAGES: 58
14. MONITORING AGENCY NAME & ADDRESS (if different from Controlling Office)	15. SECURITY CLASS. (of this report): Unclassified
	15a. DECLASSIFICATION/DOWNGRADING SCHEDULE

16. DISTRIBUTION STATEMENT (of this Report)

Approved for public release; distribution unlimited.

17. DISTRIBUTION STATEMENT (of the abstract entered in Block 20, if different from Report)

NA

18. SUPPLEMENTARY NOTES

The view, opinions, and/or findings contained in this report are those of the author(s) and should not be construed as an official Department of the Army position, policy, or decision, unless so designated by other documentation.

19. KEY WORDS (Continue on reverse side if necessary and identify by block number)

Shear Bands
Temperature Measurements,
High Strain Rates,
Stress-Strain Behavior,
Steels

per S.

20. ABSTRACT (Continue on reverse side if necessary and identify by block number)

A torsional Kolsky bar (split-Hopkinson bar) was used to deform tubular specimens of AISI 1018 cold rolled steel and AISI 1020 hot rolled steel at a nominal strain rate of 10^3 s^{-1}. Shear bands were observed to form in both steels and the temperature of the material in the bands was measured by determining the infrared radiation emitted at the metal surface. For this purpose, a linear array of ten indium-antimonide detectors was used to determine temperature history at ten neighboring points lying across the projected path of the shear

DD FORM 1 JAN 73 1473 EDITION OF 1 NOV 65 IS OBSOLETE

UNCLASSIFIED

SECURITY CLASSIFICATION OF THIS PAGE (When Data Entered)

20. (continued)

band. Results showed that shear bands in these low carbon steels are relatively wide, that the maximum temperature rise in the band is about 450°C and that the temperature distribution across the band is consistent with results based on an analysis performed by Shawki and Clifton. The two steels have very different work hardening rates and the strain at which localization is first observed is very different for the two steels: in the cold-rolled steel it occurs at about 15% strain, while in the hot-rolled the strain is nearer 100%. This result also is consistent with predictions based on the analysis.

Abstract

A torsional Kolsky bar (split-Hopkinson bar) was used to deform tubular specimens of AISI 1018 cold rolled steel and AISI 1020 hot rolled steel at a nominal strain rate of 10^3 s^{-1}. Shear bands were observed to form in both steels, and the temperature of the material in the bands was measured by determining the infrared radiation emitted at the metal surface. For this purpose, a linear array of ten indium-antimonide detectors was used to determine temperature history at ten neighboring points lying across the projected path of the shear band. Results showed that shear bands in these low carbon steels are relatively wide, that the maximum temperature rise in the band is about 450°C and that the temperature distribution across the band is consistent with results based on an analysis performed by Shawki and Clifton. The two steels have very different work hardening rates and the strain at which localization is first observed is very different for the two steels: in the cold-rolled steel it occurs at about 15% strain, while in the hot-rolled the strain is nearer 100%. This result also is consistent with predictions based on an analysis.

Measurement of the Temperature Profile During Shear Band Formation in Steels Deforming at High Strain Rates

INTRODUCTION

Adiabatic shear bands are narrow zones of highly non-homogeneous deformation that form by a thermo-mechanical instability process and frequently accompany the dynamic deformation of materials. These bands can occur during tensile, compressive or shear loading and often act as sites for the initiation and propagation of fracture (Figure 1). They are important in a diverse series of applications including machining, ballistic impact and high velocity shaping and forming. Recently, much has been learned about adiabatic shear band formation from a number of experimental and analytical studies. For instance, it is generally accepted that shear bands nucleate due to the presence of a local inhomogeneity or defect, causing enhanced local deformation and local heating. Once non-uniform flow begins, the deformation will become increasingly unstable as straining continues if the heat that is produced during deformation is given insufficient time to be conducted away.

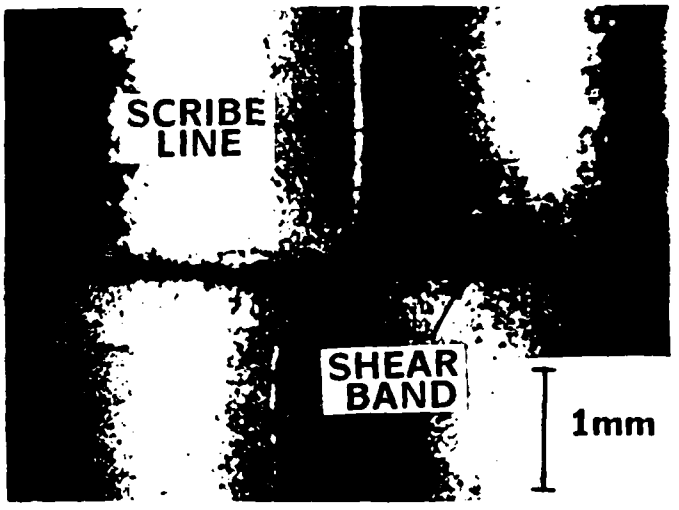

Figure 1: Shear Band and Partial Fracture in AISI 1018 Cold Rolled Steel (Specimen No. 96)

Localization occurs more readily in materials with a low strain hardening rate, a high strain rate sensitivity, a low thermal conductivity and a high thermal softening rate. Bands also form readily in high strength materials where, presumably, the heat due to deformation is greater for a given plastic strain increment. Reviews of the subject have been presented by Rogers [1, 2], Hutchinson [3], Olson, Mescall and Azrin [4], Clifton [5] and Bedford, Wingrove and Thompson [6]. At present, despite a number of excellent studies, many aspects of shear band development are relatively unexplored and a large amount of additional research is necessary before a full understanding of the details of strain localization into shear bands can be gained.

Analytical Studies

A number of analytical studies have been performed in attempts to determine the critical conditions for the onset of an instability during deformation. In most of the models, the material is taken to be a continuum with some form of initial inhomogeneity and the effects of material properties such as strain hardening, thermal softening, and strain rate sensitivity on behavior are examined. For a rigorous evaluation, the fully coupled heat and deformation equations must be solved simultaneously. In general, in experiments during which a shear band forms, the flow stress is seen to reach a maximum after which it decreases with further deformation. This maximum is often taken to represent the onset of nonuniform flow, and many researchers, including Basinski [7], Recht [8], Argon [9], Culver [10] and Staker [11], have developed localization criteria that depend on the flow stress maximum in the adiabatic stress-strain curve. Costin, Crisman, Hawley and Duffy [12] and Merzer [13] present computer simulations of thin-walled tubes in torsion identical to those used in the Kolsky bar experiments. Clifton [5] examined the stability of a quasi-static simple shear deformation using a linear perturbation method. His analysis included strain hardening, thermal softening, heat conduction and strain rate effects. Bai [14] performed a similar

perturbation analysis which included the effects of inertia. Both the Clifton and the Bai analyses are limited by the assumption of constant coefficients in the linearized equations that are evaluated from the homogeneous solution. Fressengeas and Molinari [15] examined thermal and inertial effects during uniaxial tension using a one-dimensional model. Another numerical simulation of the Kolsky bar tests, detailed in Shawki, Clifton and Majda [16] and in Clifton, Duffy, Hartley and Shawki [17], examines the effect of three different visco-plastic constitutive equations and the choice of velocity or of stress boundary conditions on the numerical solution of the simple shear problem. In this analysis a linear perturbation is used to solve the full set of nonlinear equations, including time-varying coefficients. In addition, the explicit solution of the linearized equations with constant coefficients is determined. This model, when employed with a power-law constitutive equation, provides good agreement with the results of Kolsky bar experiments in 1018 cold-rolled steel and in 1020 hot-rolled steel, and will be discussed in more detail later in this report. A different approach to the localization problem from those described above is taken by Wu, Toulios and Freund [18], who examine initiation and crack-like propagation of shear bands from a local defect during anti-plane shear deformation.

It is apparent from the above analyses that the particular constitutive relation chosen has considerable bearing on the predictions based on the analytical model. Perhaps when more experimental evidence becomes available as to the material factors that act to nucleate a shear band and when results are obtained about the growth of inhomogeneous strain and of the temperature profiles during deformation, a better understanding will be gained of the parameters that need to be included for the development of models that predict more accurately the tendency to shear banding. In addition, experimental results obtained during deformation should make more evident the relative importance of the various material properties and thus lead to a more comprehensive understanding of the instability process.

Experimental Studies

Most experimental data on shear bands are obtained by measurements and observations made on the specimen after testing is completed. The lack of data acquired during the process of shear band initiation and growth is due primarily to difficulties inherent in the experiment. The nearly-adiabatic conditions necessary for shear band formation generally require high strain rate deformation, and the resulting shear bands may form in a matter of microseconds. They propagate rapidly through the specimen, often are as narrow as a few microns, and frequently are followed by fracture almost immediately after their formation. This combination of high speed and narrowness makes it difficult to obtain any detailed measurements of band width, of strain distribution or of temperature distribution during shear band formation. Yet, these are precisely the measurements of most value in any comparison with predictions of analyses. To the above experimental difficulties should be added the fact that the investigator generally does not know precisely when or where the shear band will form within the specimen.

As a result of these fairly severe experimental problems, most investigators focus on obtaining only overall values of stress, strain and strain rate, and supplement these by observations and measurements made of the metal after the test has terminated. To date, this type of observation has provided nearly all experimental knowledge about the formation and characterization of shear bands and their structure. One exception is found in the tests of Costin et al. [12], who measured shear band temperature during testing and found that the local temperature within the band is much higher than in the homogeneously deformed material to either side of it. The purpose of the present paper is to refine the experimental technique of Costin et al. in order to obtain more accurate values of temperature and to obtain the temperature distribution within the shear band.

THE EXPERIMENTAL METHOD

Torsional Kolsky Bar

The tests described in this report were performed in the torsional Kolsky (split-Hopkinson) bar, shown schematically in Figure 2. The basic apparatus was developed by Kolsky [19] for compressional loading at high strain rates. Later investigators modified the apparatus for testing in torsion, [20-22]. Torsional loading is advantageous for the study of shear bands because there is no change in the cross-sectional area of the specimen during deformation due to necking or barrelling as occurs in tensile or compressive loading at higher strains. In addition, the advantage of the Kolsky bar over methods such as impact or expanding cylinder testing is that the average strain rate and the average strain can be controlled more easily.

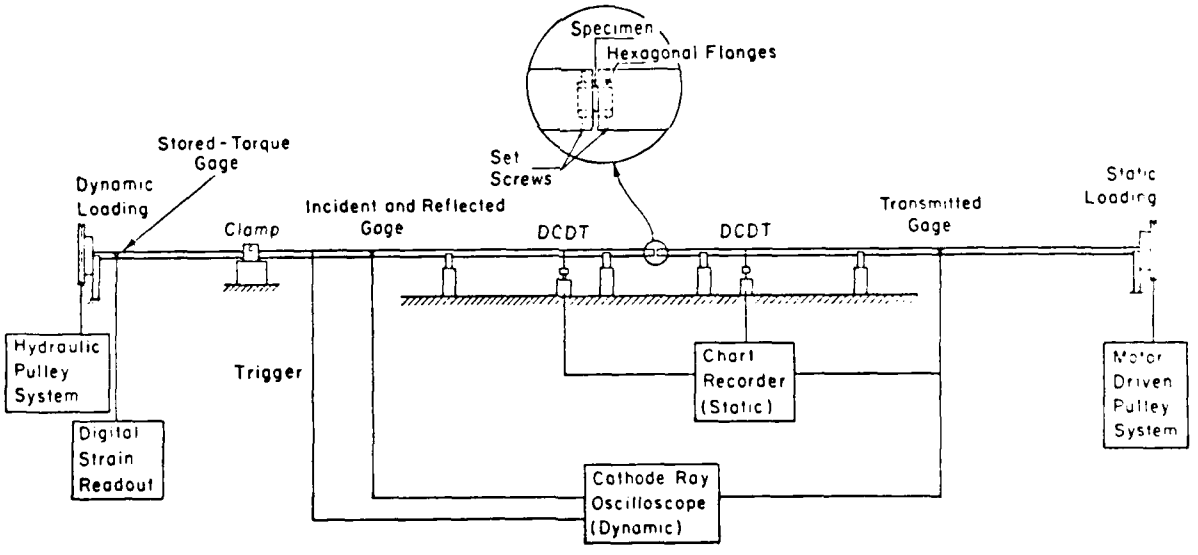

Figure 2: Schematic of the Torsional Kolsky Bar

The Kolsky bar used in the present experiments is made of 6061-T6 aluminum alloy 25.4 mm (1.0 in) in diameter that is supported along its length by a series of Teflon bearings. The high strain rates are achieved through the sudden release of a stored-torque at one end of the

Kolsky bar, thus initiating a torsional pulse. Electric resistance strain gages measure the magnitude of this stored-torque, whose sudden release is effected by fracturing a brittle breaker-piece that forms part of the clamp. Upon release of the torque, a sharp-fronted torsional loading pulse of constant amplitude (equal to half the stored torque) propagates down the bar toward the specimen. Simultaneously, an unloading pulse of equal magnitude propagates from the clamp toward the torque pulley. The mechanical impedance of the pulley is sufficiently large so the unloading pulse, after reflection from the pulley, reduces the torque in the incident bar to zero as it propagates toward the specimen. The duration of the loading pulse at the specimen, therefore, is the time required for a pulse to travel twice the distance along the bar between clamp and torque pulley. The rise-time of the loading pulse produced with the present apparatus is about 40 microseconds and the duration of the pulse can be varied by changing the position of the clamp along the bar.

Strain gages are mounted on the incident and transmitter bars, the former to measure the incident and reflected pulses and the latter the pulse transmitted through the specimen. Their location along the bars must meet two requirements. First, the gages on the incident bar must be far enough from the specimen to avoid overlap between the incident and reflected pulses. In addition, the gages on the incident and transmitter bars must be mounted at the same distance from the specimen, if Lindholm's method [23] is to be used to convert their outputs into a stress-strain diagram for the specimen material. At each station, two four-arm electric resistance strain gage bridges are mounted with the gages sensitive to strain at 45° to the bar's axis. The signals from the gages during testing as well as during calibration are recorded in a Nicolet 4-channel digital oscilloscope. As shown by Kolsky, the average strain and stress in the specimen can be inferred, respectively, from the measured records of the strain in the incident and transmitter bar. The reflected pulse provides a measure of the average shear strain rate in the specimen, $\dot{\gamma}(t)$, and, through a single integration, provides the average shear strain in the specimen, $\gamma(t)$. The magnitude of the

pulse transmitted through the specimen is a direct measure of the average shear stress in the specimen, $\tau(t)$. Details of these calculations and a more thorough description of the torsional Kolsky bar can be found in reference [24]. A schematic diagram of the output from the incident and transmitter bar gages and the oscilloscope output from a typical test are presented in Figure 3. It must be emphasized that, when interpreting the records, the strain and strain rate are obtained from the relative rotation of the two ends of the specimen. Hence, they represent only average values over the gage length of the specimen and do not provide information about the distribution of the strain or strain rate across the gage section. Thus, when a shear band forms, the strain given by these records will be an average over both the highly strained shear band region and the area outside the shear band. However, since the strain within the shear band is considerably greater than that in the remainder of the gage length, the output of the strain gages can provide some estimate of the shear band strain.

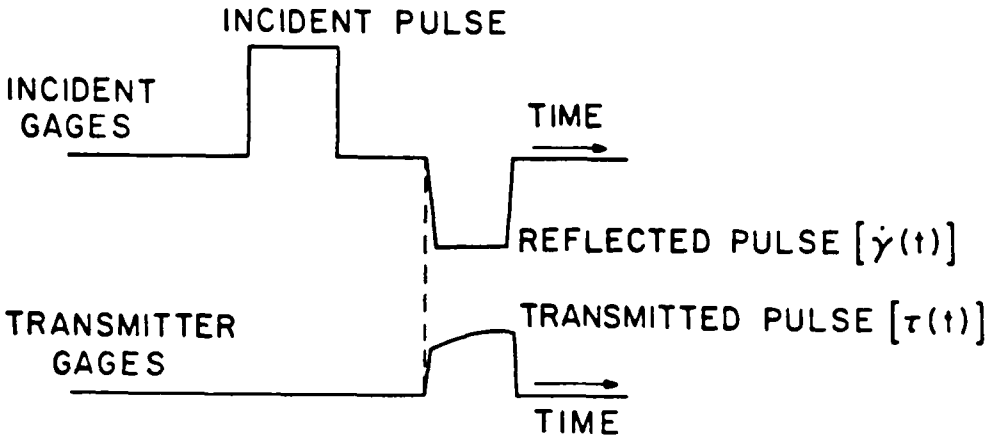

(a)

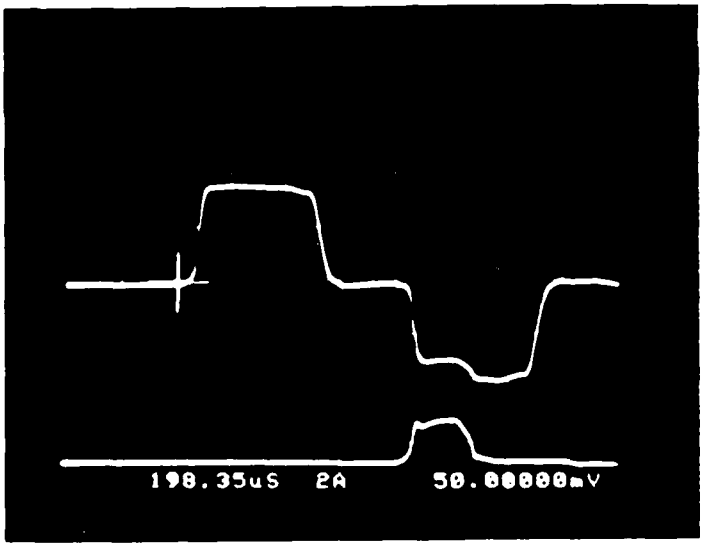

(b)

Figure 3: Gage Output from Torsional Kolsky Bar. (a) Schematic and (b) Oscillograph from a Typical Test.

Specimens

The specimen used in the torsional Kolsky bar is a thin-walled tube with integral hexagonal flanges machined from bar stock (Figure 4). Its flanges fit into matching hexagonal sockets in the Kolsky bars. The dimensions of the hexagonal flanges are chosen to provide the same torsional impedance as the aluminum Kolsky bars. Indeed, by means of a separate test it was shown that there is no pulse reflection at the flanges. In addition, to assure no lost motion between the sockets and the flanges, a set of 12 small set screws in each socket is used to hold the specimen's flanges against the driving faces of the hexagonal sockets.

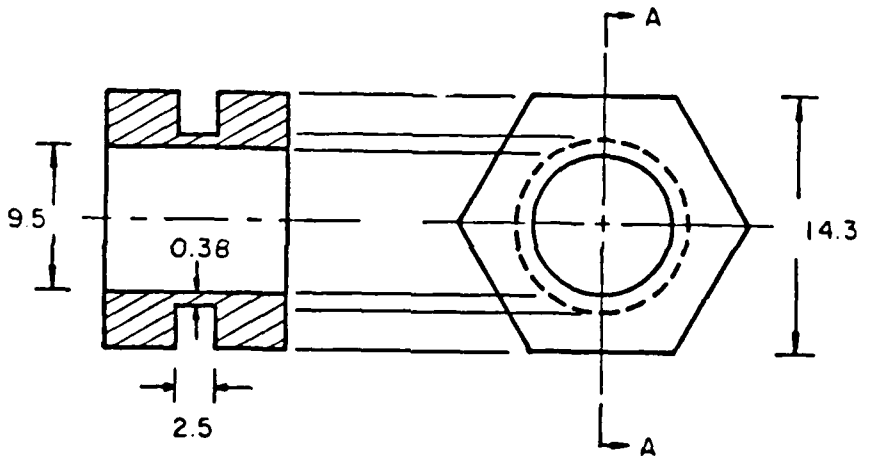

Figure 4: Specimen Used in the Torsional Kolsky Bar Experiment (All Dimensions are in Millimeters)

The specimen proper is the short tube between the two flanges (Figure 4). It has a gage length of 2.5 mm (0.1 in), an internal diameter of 9.5 mm (0.375 in) and a wall thickness of approximately 0.4 mm (0.015 in). The inside and outside walls of the tube are given a fine polish prior to testing to remove defects due to machining. In order to determine the final permanent strain distribution in the specimen, fine lines are scribed at equal intervals

around the inside wall of the specimen parallel to its axis. The slope of these lines after deformation represents the final permanent strain across the gage section. As shown by Costin et al. [12], in the case of a homogeneous strain distribution the inclination of these lines is constant along the gage length of the specimen (Figure 5a) with their angle equal to the final shear strain. If the final strain distribution is inhomogeneous, the slope of the scribe lines will no longer be constant and a large inclination will result in the region of high local strain (Figure 5b). By measuring the angle of inclination, a direct measure of the final permanent strain profile within a shear band can be determined. In the present investigation the specimen materials studied were AISI 1018 cold rolled steel (CRS) and AISI 1020 hot rolled steel (HRS).

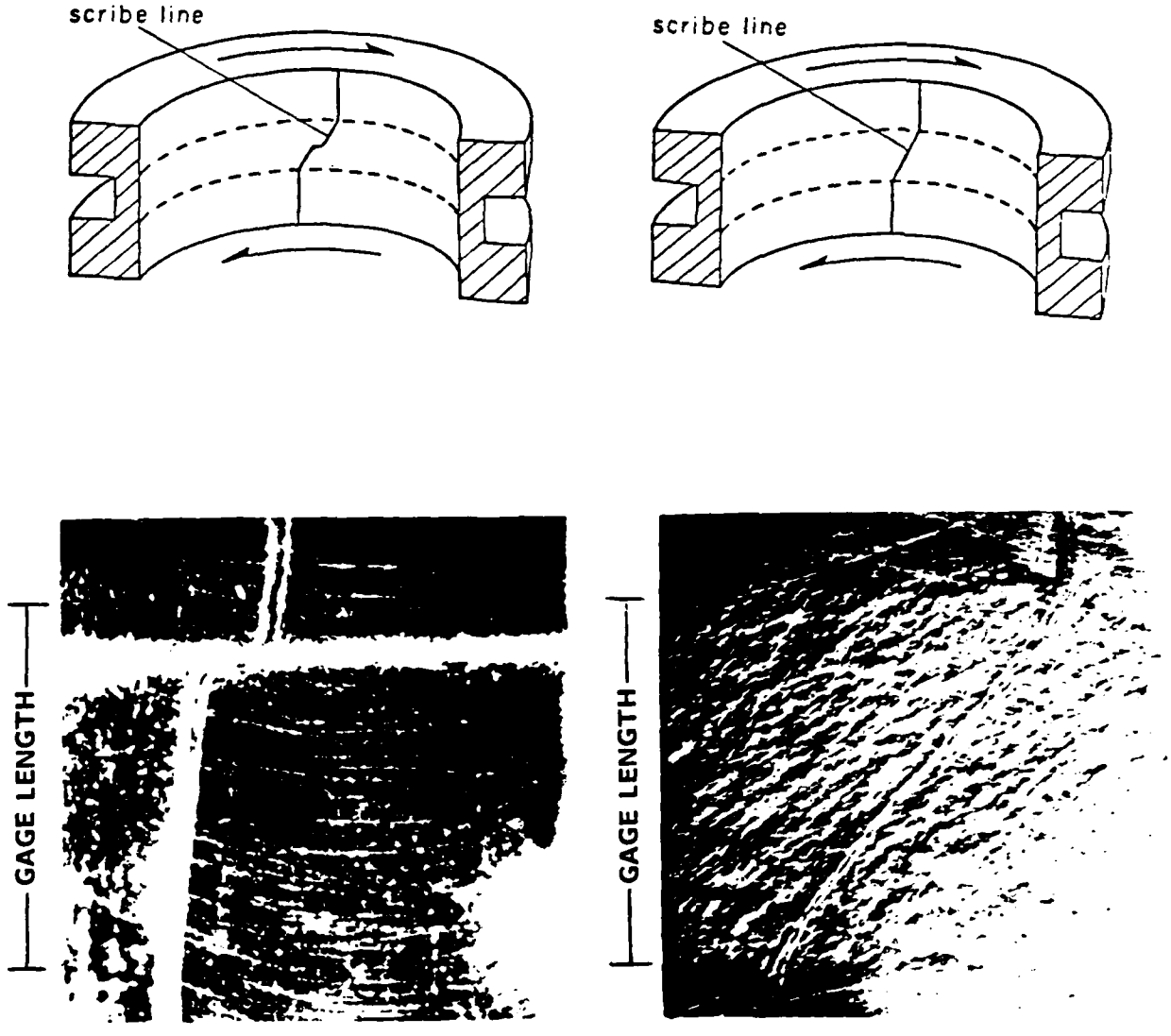

Figure 5: Sectioned Specimens Showing Scribe Line After Deformation. (a) 1018 CRS Specimen with Shear Band and (b) 1020 HRS Specimen Showing Homogeneous Deformation; (ref. Costin et al. [7]).

Infrared Radiation

In general, the thermal radiation emitted by a body will cover a broad continuum of wavelengths. For an ideal blackbody, the intensity of the radiation is a function of its temperature and not of the material. For a real material, however, the power emission density , W, is less than that of a blackbody, W_B, and the ratio W/W_B is known as the emissivity, ϵ. Planck's law describes the spectral dependence of blackbody radiation in terms of the velocity of light, c_L, the Boltzmann constant, k, and the quantum of radiant energy, $h\nu$, where h is Planck's constant and ν the frequency of the radiation. The emission density for blackbody radiation of wavelength λ at temperature T (°K) was shown by Planck to given:

$$W_B(\lambda, T) = \frac{2\pi hc_L^2}{\lambda^5 [\exp(hc_L/\lambda kT) - 1]}$$

as shown plotted in Figure 6. Integrating this expression over the range of wavelengths gives the total emission density:

$$W_B = \sigma T^4$$

where σ is the Stefan-Boltzmann constant. It can be seen from Figure 6 that the spectral emittance is zero at very short and very long wavelengths and passes through a maximum at a wavelength λ_{max}. At higher temperatures, the wavelength at which this maximum occurs becomes shorter. By differentiating Planck's formula and locating the maximum, it can be shown that:

$$\lambda_{max} = c_3/T$$

where the constant, c_3 equals 2898 micron per degree absolute. This formula is useful even for real bodies, since it gives an approximate value of the peak radiation wavelength for any temperature. The total blackbody emission density, W_B, which is given by the area under the curve, increases rapidly with temperature and its peak shifts toward shorter wavelengths. For a real body, the results could be corrected for the reduced emissivity, ϵ.

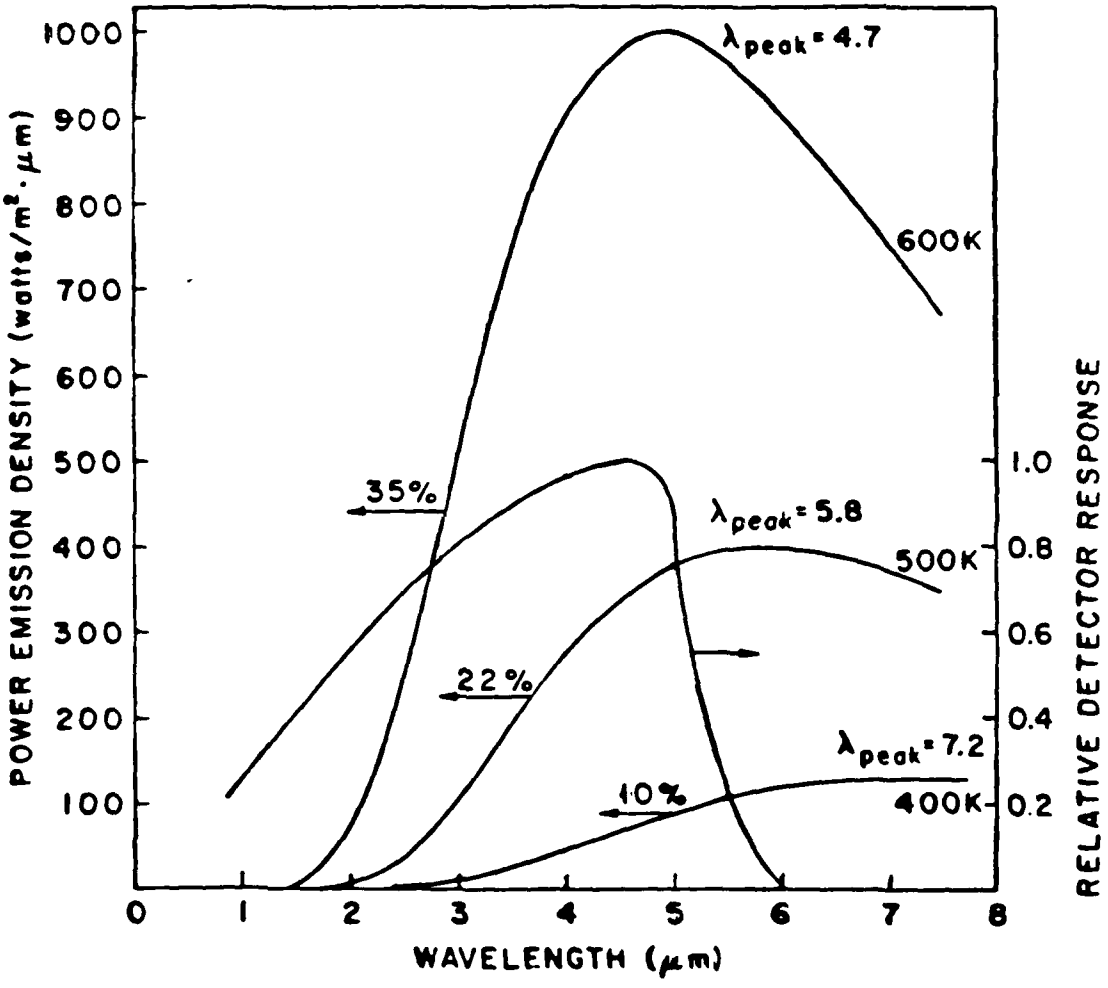

Figure 6: Power emission density W_B as a function of wavelength λ Derived from Planck's Law for a Blackbody. Also shown in this figure is the response of the indium-antimonide detector, and the percentage of the total emission density to which indium-antimonide is sensitive.

Infrared Radiation Detection

Measuring the emitted infrared radiation during testing has proven to be a convenient method for determining the temperature of a developing shear band [12]. The advantages of this technique are its rapid response time (less than 100 nanoseconds) and the fact that it requires no physical contact with the deforming body. Since the detector elements are small, the optical system can be designed to control the magnification of the system and hence measure temperature over different spot sizes on the specimen. These advantages are especially important in the study of shear bands, where high temperatures may develop in microseconds. In addition, the rapid response is critical because heat conduction to the cooler metal on either side of the band is much greater than the heat loss to the air, and will cause the temperature to fall off rapidly as the deformation ceases.

A number of researchers have applied infrared radiation detection to measure the temperature increase due to plastic work during straining. Hayashi, Yamamura and Okano [25] used an indium-antimonide single element detector to find the surface temperature increase during plastic deformation in a number of metals. Moss and Pond [26] employed a copper–doped germanium semiconductor crystal to detect the radiation emitted by copper samples during elongation. They found abrupt changes in emisssion that correlated with the intermittent plastic deformation during the formation of Luders bands. Using a calibration that accounted for the variation of surface finish within their temperature range, they found a temperature difference of 0 to 18 °C across the boundaries of the Luders bands. Costin et al. [12] used an infrared radiation technique to examine inhomogeneous deformation in the form of shear bands in AISI 1018 cold rolled steel. By focussing on a spot 1.0 mm wide with a spherical mirror they were able to measure the temperature at one spot with a single element detector during torsion tests at a nominal shear strain rate of

500 sec^{-1}. According to their results the temperature at the shear band increased by 60 or 100°C due to the enhanced plastic deformation occurring there [27]. However, because the area over which they measured the radiation is more than twice as wide as the shear band itself, their results undoubtedly underestimate the actual temperature rise. In all these studies, an infrared detection system is applied successfully to measure the temperature increase at one spot on a deforming body. By using a multiple element detector as described below, it is possible to look at the temperature profile as it develops across a specimen, and to understand better the nature of inhomogeneous deformation.

The detector used in the tests to be described in this report is a ten-element system constructed by Judson Infrared. It consists of a linear array of ten individual indium-antimonide (InSb) cells mounted on a Dewar flask cooled with liquid nitrogen to 77°K (Figure 7). The choice of material for the detector elements depends on the spectral response needed for a particular temperature range, as well as on the required response time of the system. InSb responds to radiation in the 0.5 to 5.5 micron range, which is adequate for the measurement of shear band temperatures. It is conveniently used in the photo-voltaic mode to give a response time of less than a microsecond, which easily meets present needs. When cooled with liquid nitrogen, the performance of InSb improves by an order of magnitude due to higher responsivity, longer wavelength sensitivity and decreased thermal noise. Each of the elements in the detector array is rectangular with a width of 0.41 mm (0.016 in) and a height of 1.63 mm (0.064 in). The separation between the elements on the detector plane is 0.13 mm (0.005 in). By using a linear array of ten elements, temperature measurements can be effected at ten spots across the specimen gage section simultaneously, each as a function of time. The output of each element is individually amplified and recorded on one channel of an oscilloscope. A typical output is shown in Figure 8.

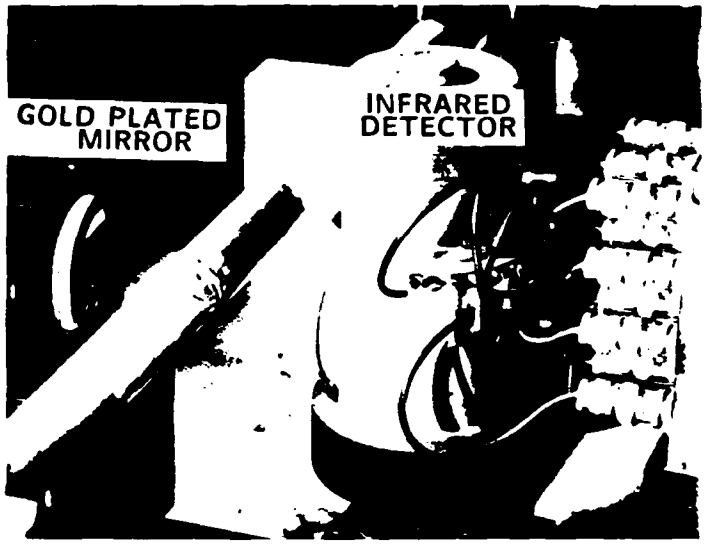

Figure 7: Photograph of InSb Detector-Mirror System Showing I-R Detector, Spherical Mirror and Kolsky Bar. Distances Are Not Those Used for an Actual Test.

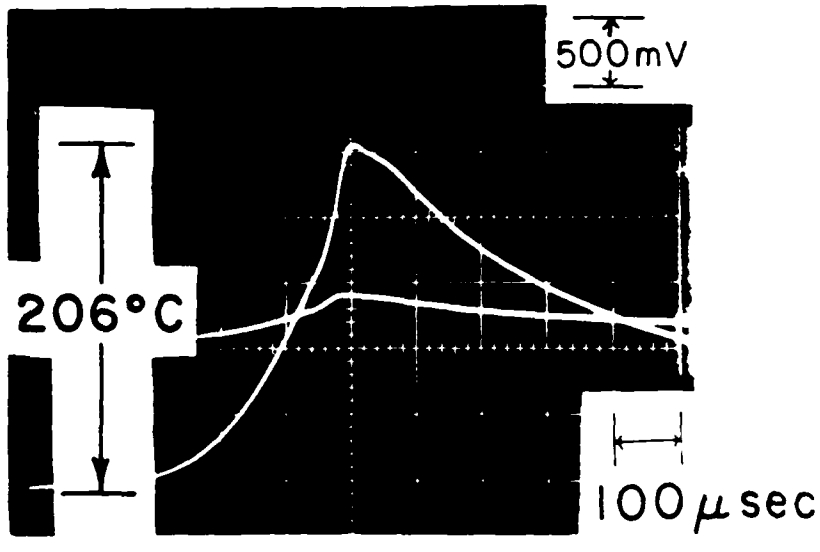

Figure 8: Typical Output From a Detector Element.

The Optical System

The infrared radiation emitted from the specimen surface was focussed onto the detector array by means of a gold plated spherical mirror, Figure 9. The reason for choosing a mirror rather than a lens was to avoid the chromatic aberration that results from the differences in the optical path as a function of wavelength due to lens refraction. This is particularly important in the case of infrared radiation where the range of wave lengths is relatively broad. In addition, with a mirror it is possible to use visible light to focus the system. The spot size viewed by each detector element (the magnification) was controlled by adjusting the optical distances between the specimen, the mirror and the detector elements. Besides spherical aberration, astigmatism and coma occur when rays deviate considerably from the axis of symmetry of the mirror. Unfortunately, for the present tests it is necessary to position the detector slightly off-axis to avoid shading of the output by the Kolsky bar and specimen. Although, every attempt was made to reduce aberrations by keeping the specimen and detector array as close to the optical axis as possible without blocking the image, some distortion can not be avoided.

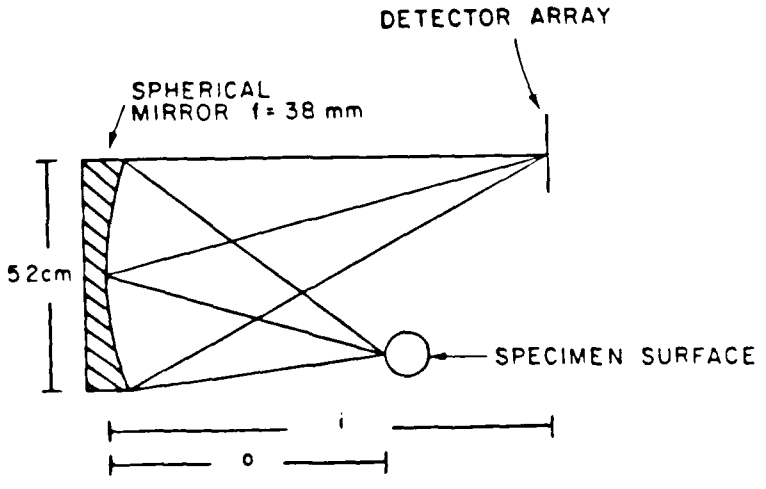

Figure 9 Schematic Diagram of Optical Arrangement (Not to Scale). Dimensions o and i Are Varied to Change the Spot Size on the Specimen.

Any optical system is limited in its resolution, and for a mirror of diameter D, of focal length f, the approximate diameter of the smallest resolvable spot, d, is given by

$$d = 1.22 \lambda \, f/D$$

where λ is the wavelength of the radiation. For our mirror, f = 38 mm and, if D = 52 mm, then:

$$d = 0.89 \lambda$$

For example, for a wavelength of 5 microns the smallest resolvable spot will be 4.5 microns in diameter. This is important when a large magnification is used to look at a small area on the specimen. The smallest spot width used in the present tests is 20 microns.

Focussing

Before each test, the detector-mirror system was focussed to obtain a sharp image of the specimen gage section on the element array. For this purpose, the specimen was replaced in the bar by a dummy specimen of precisely the same dimensions but with a small hole in the center of its gage section. The diameter of the hole was approximately 0.44 mm (0.018 in) and its axis was normal to the specimen's surface, (Figure 10). A 0.05 mm (0.002 in) wire was positioned across the hole and a small bulb placed inside the specimen to project the image of the wire onto the element array.

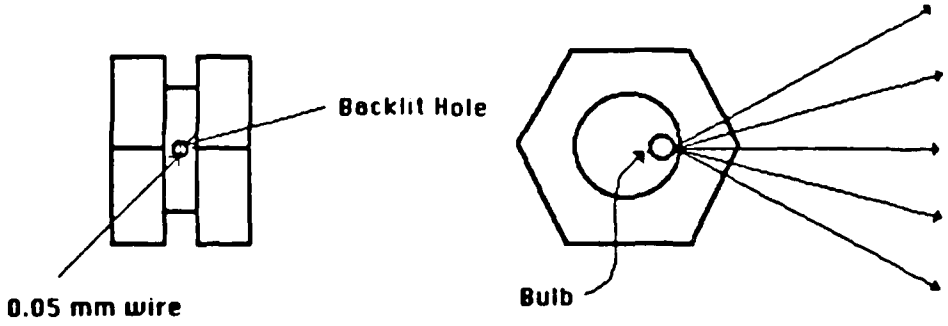

Figure 10: Dummy Specimen Used for Focussing I-R Detector-Mirror System.

Since each detector element is 0.41 mm (0.016 in) wide, the width, s, of the spot observed on the specimen corresponding to each element is given by:

$$s = 0.41/M$$

where M is the magnification and s is expressed in millimeters. When the dimensions are adjusted so M = 1.6 then s = 250 microns, while for M = 20, s = 20 microns. Fine adjustments were made by resolving the image of the wire to obtain the best focus on the element array. After the focussing was complete, the dummy specimen was replaced by an actual specimen in precisely the same location.

Calibration and the Effect of Surface Finish

The detector-mirror system was calibrated before and after every series of tests. The first step in the calibration process is to measure the infrared radiation emitted from an undeformed specimen heated internally with a soldering iron. The temperature of the calibration specimen is measured simultaneously by using a thermocouple imbedded in the gage section. Temperature and detector output readings were recorded at temperature increments of 10°C starting at room temperature, heating to the maximum possible temperature and then cooling to room temperature, Figure 11. A rotating notched disk between the mirror and the detector was used to chop the output and produce an AC signal. Each element of the detector was calibrated separately and the response of the ten elements was found to be almost identical, with the output increasing rapidly at the higher temperatures. An additional check was made to determine the amount of cross-talk between elements, i.e. the output of an element due to radiation on adjacent elements. For this purpose a thin wire was heated and passed in front of the detector face. When the maximum output was reached at one element, indicating that the wire was positioned in front of it, the output of the adjacent elements was recorded. It was found that the effect of cross-talk on the signal from the adjacent

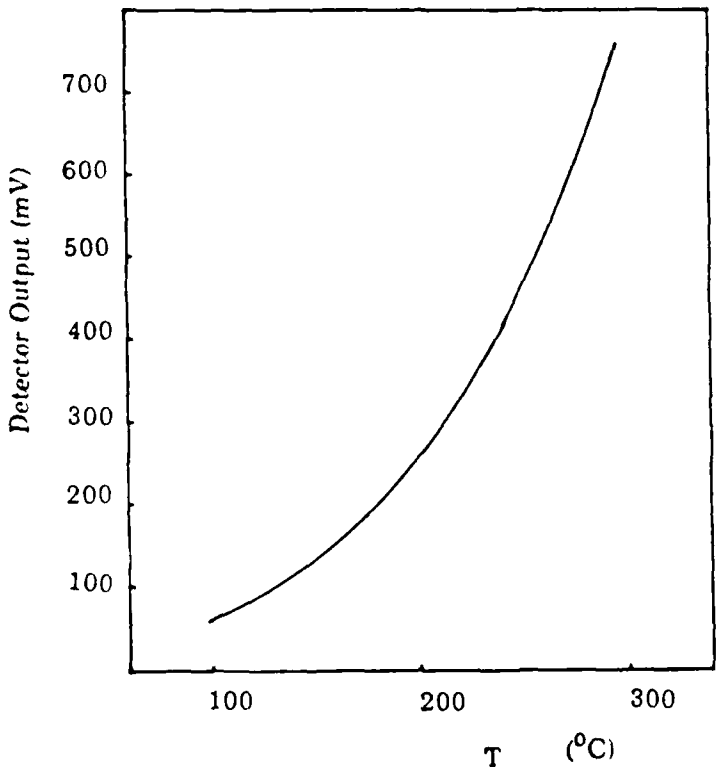

(a)

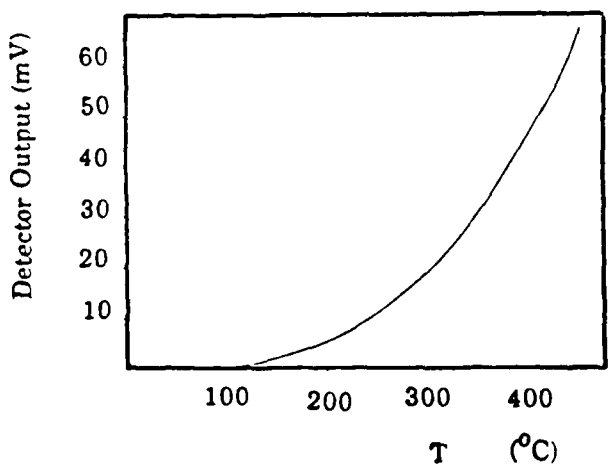

(b)

Figure 11: Calibration Curves for Two Magnifications. (1) 250 micron Spot Size and (b) 20 micron Spot Size.

elements is about ten percent of the output of the element on which the radiation was focussed. The test results presented here were not adjusted to account for cross-talk.

When polished steel specimens are subjected to a large shear strain, the initial surface finish is destroyed and the surface acquires a mottled appearance. In particular, if the strain localizes into a shear band, there is a visible difference in surface finish between the material inside and outside the band. To determine whether the effect of the variation in appearance on the emitted infrared radiation is significant in these tests, two separate checks were made during the calibration. First, both a polished specimen and a specimen that had been strained quasi-statically to a uniform strain of over 150 percent were calibrated separately using the method described above, Figure 12. It can be seen that while there is a difference in output between the two specimens at the lower temperatures, the two curves merge as the temperature increases. Thus, although at a low enough temperature the emissivity change may become pronounced, for the range of temperatures expected during shear band formation the effect of the change in surface finish is insignificant. In addition, because the strains within the shear band are actually much higher than the 150 percent imposed quasi-statically, a further check was made. A CRS specimen, previously deformed dynamically and containing a shear band, was heated internally and scanned by the detector to determine if there was a change in output near the shear band. Again it was found that the mottling that occurs due to the large strain at the shear band has little to no effect on the emitted radiation in the range of temperatures that is important for these tests. At lower temperatures this effect may become significant, as was seen by Moss and Pond [26].

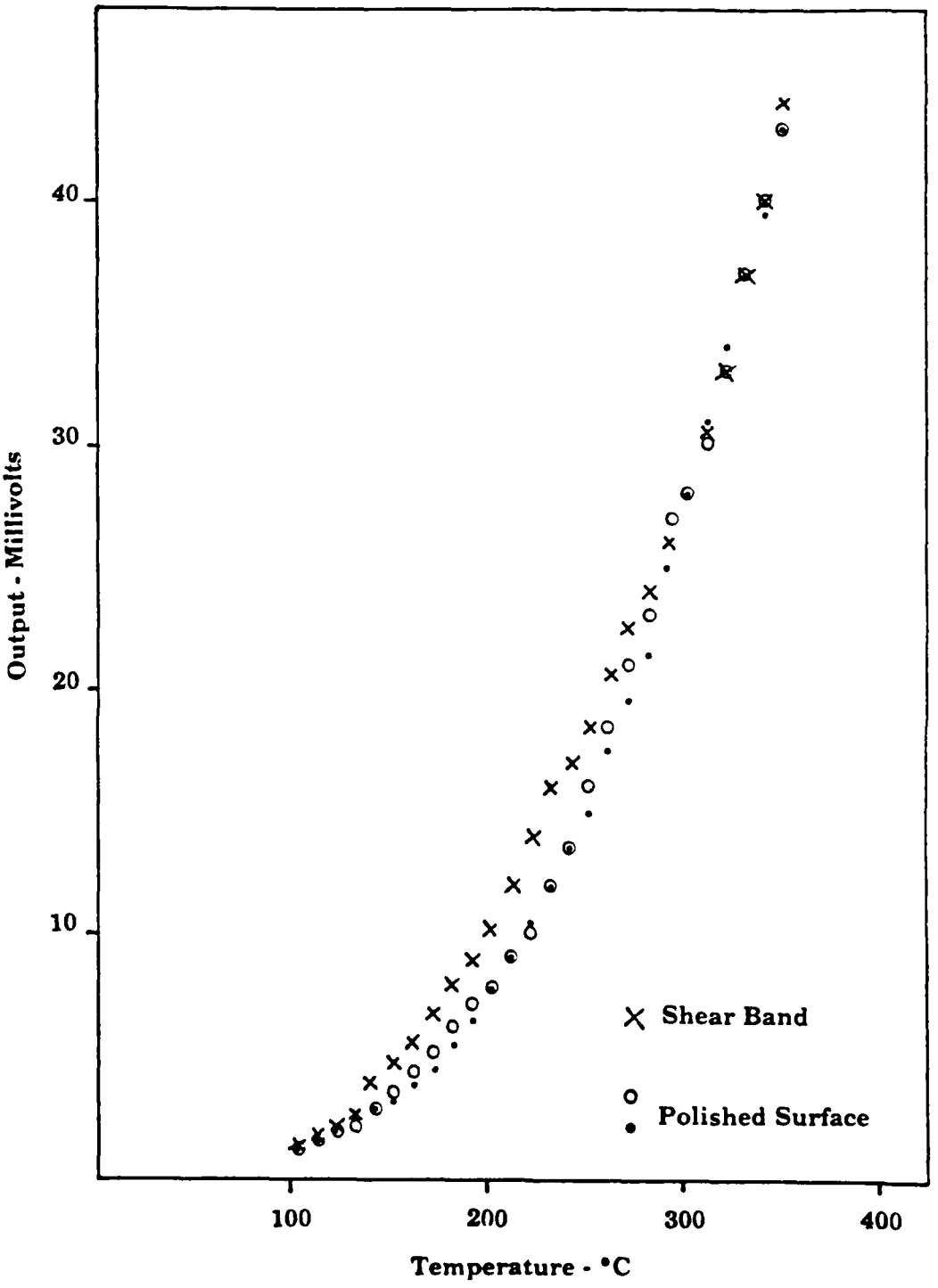

Figure 12: Calibration Curves Showing Surface Finish Effect.

Metallurgical Examination of the Specimens

Many of the specimens tested were examined metallurgically using optical microscopy to determine microstructure before and after etching and scanning electron microscopy (SEM) was used to examine fracture morphology and detailed structure. For optical microscopy, specimens were sectioned with a spark cutter and potted in epoxy. They were then polished using three grades of wet emery paper and finished on polishing wheels saturated with a 0.05 micron suspended alumina solution. After polishing, the specimens were etched with a nital solution and examined microscopically. The SEM observations were performed using an AMR 1000A Scanning Electron Microscope, with which it is possible to obtain high resolution photographs of the fracture surface. All specimens observed in the SEM were stored in a vacuum for the brief period between testing and microscopy to reduce corrosion, and were unetched. All specimens were cleaned in an ultrasonic bath prior to SEM analysis.

RESULTS OF TESTS WITH AISI 1018 COLD ROLLED STEEL

This section presents the results of tests in which shear band temperature was measured in specimens of AISI 1018 cold rolled steel (CRS). Its composition is given in Table 1. Cold rolled steel is a particularly attractive metal to test because relatively wide deformed shear bands form at strains of only 10 - 20 percent. These bands are about 0.25 mm (0.01 in) in width and hence relatively easy to detect. Two series of tests were performed with differing optical arrangements in order to be able to focus the infrared detectors on larger and smaller spot sizes on the specimens. For the first series, the 0.250 mm (250 micron) spot size was used as described in the preceding section. Since ten separate spots are observed on the specimen, this allows for measurements across the entire gage section of the specimen (2.5 mm). The width of this spot equals approximately that of the deformed shear band, and hence provides only an average temperature for the band. However, a comparison can then be made with the temperature increase calculated from the plastic work of deformation. In addition, further tests were conducted using a 20 micron spot size. Since the distance between spots at this magnification is 8 microns, this allows for a measurement of the temperature profile across the shear band. The highly non-homogeneous strains that occur within the bands suggest that the temperature distribution is not uniform, and this was confirmed by the temperature measurements. These measured values of temperature were compared with predicted values based on the analysis of Shawki and Clifton [16], [17], [28], in which a thin-walled tube, presumed to have an initial imperfection, is deformed in torsion.

Mechanical Behavior

A list of the tests performed with the CRS is presented in Table 2, and a typical stress-strain curve in Figure 13. It was found that a shear band formed in every test performed with this steel, and that the flow stress during testing always

Table 1: 1018 CRS: Chemical Composition (Weight Percent)

C	Mn	P	S
0.18	0.71	0.020	0.022

Table 2: List of Tests Performed with 1018 CRS

Spec No.	$\dot{\gamma}$ sec^{-1}	γ_{max} %	τ_y MPa	τ_{max} MPa	γ at τ_{max} %	Shear Band and/or Fracture	Spot size (microns)	Max $\Delta T(^{\circ}C)$
77	700	28	420	448	14	SB	250	240
81	800	24	420	450	9	SB	250	-
90	700	28	416	448	16	SB	250	206
148	1000	42	400	441	9	SB, F	20	430
151	1000	45	405	441	15	SB, F	20	235
160	1200	40	393	414	13	SB, F	20	420
164	1200	50	400	434	16	SB	20	-
165	1100	45	414	448	15	SB, F	20	420
166	1100	45	400	448	15	SB	20	235

reached a maximum value, after which the material softened until fracture or until the end of the loading pulse. In Table 2, $\dot{\gamma}$ represents the nominal or average strain rate during deformation in the plastic range and γ_{max} the maximum strain attained. The initial yield stress is designated by τ_y and the maximum value of flow stress by τ_{max}, occurring at a value of strain given in the next column. As previously mentioned, a shear band was observed in all tests with this steel and in some cases resulted in fracture as indicated by the letter F. The last column in the table gives the value of the maximum observed temperature in all tests for which the measurement was successful.

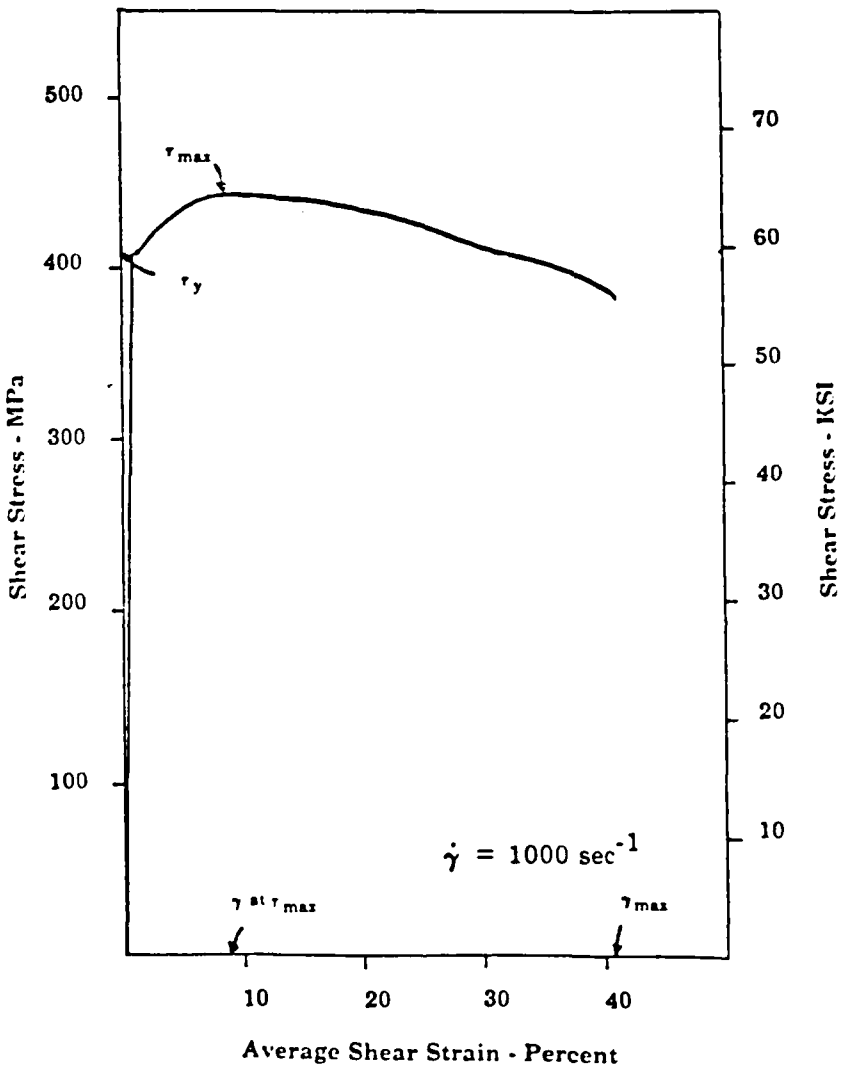

Figure 13: Shear Stress - Shear Strain Curve for 1018 CRS (Specimen No. 148)

The photograph in Figure 14 shows a CRS specimen sectioned to reveal the shear band and one of the scribe lines, which is highly inclined in the area of the band. The width of the shear band was measured at the conclusion of each test and values ranged from 0.2 to 0.3 mm. These values, however, are not precise because, as may be seen from the rounded form of the scribe line in the figure, the strain across the band is not constant, with the largest strain, about 200% in this case, near the band's center. This non-uniform strain distribution within the band was typical of present results and is quite different from the distribution observed by Costin et al. [12] with CRS, which showed a nearly constant inclination of the scribe line within the shear bands. The reasons for this difference are not immediately apparent, and all attempts to resolve this anomaly were unsuccessful. In addition, to the left of the scribe line, the photograph reveals a fine microcrack running near the center of the shear band in a direction generally parallel to the band. Cracks of this nature did not appear in all tests, as may be seen by consulting Table 2.

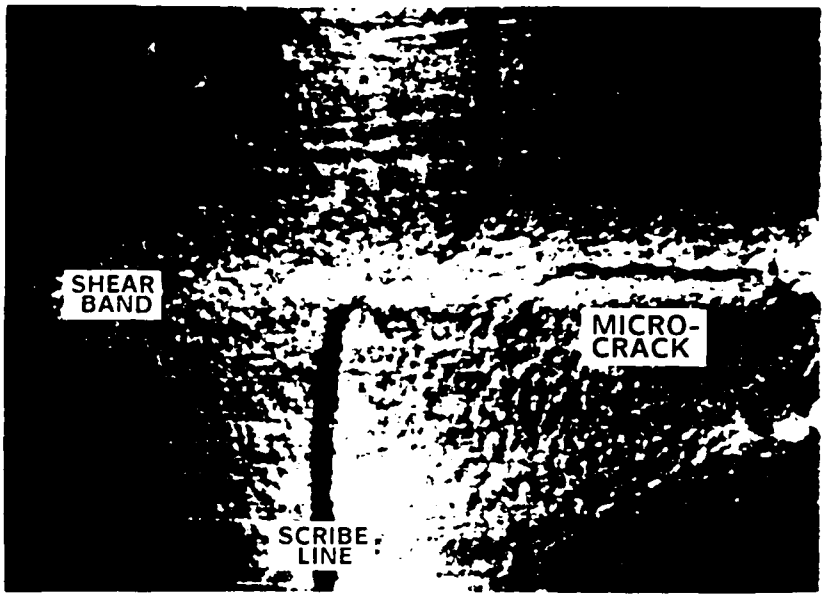

Figure 14: 1018 CRS Specimen, Sectioned After Testing to Reveal Scribe Line (Specimen 148).

When fracture occurred in a test, the path of the crack generally followed approximately the center-line of the shear band, although occasionally cracks were seen that curved away from the shear band apparently during arrest. Often specimens fractured entirely around the band's circumference. Figure 15 shows an SEM photograph of the fracture surface of a CRS specimen that first had developed a shear band. The fracture surface appears distinctly fibrous; it is made up of a series of elongated voids oriented in the direction of shearing. A study of dynamic fracture in tension by Costin, et al. [29] using the same CRS showed that at room temperature the fracture mode is one of cleavage, (although an increase of about 20°C results in ductile initiation). Hence the fibrous fracture seen in these tests indicates that some local heating probably occurred prior to fracture.

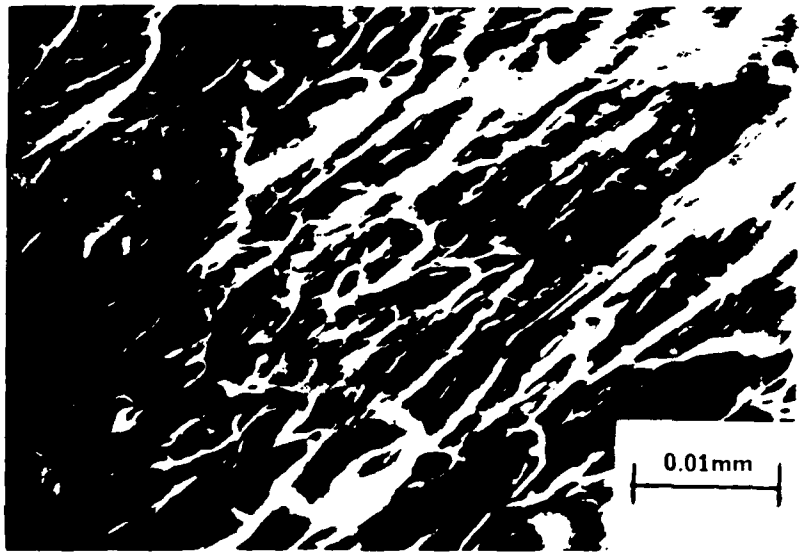

Figure 15: SEM Photograph Showing Fracture Surface of CRS Specimen (Specimen 165).

The high ductility in the shear band region can also be seen in the micrograph of the polished and etched specimen of Figure 16. The grains within the band are highly deformed relative to the surrounding metal, with a strain near the center of the band in excess of 500%. A closer examination of the shear band material in comparison to the undeformed microstructure is shown in Figure 17.

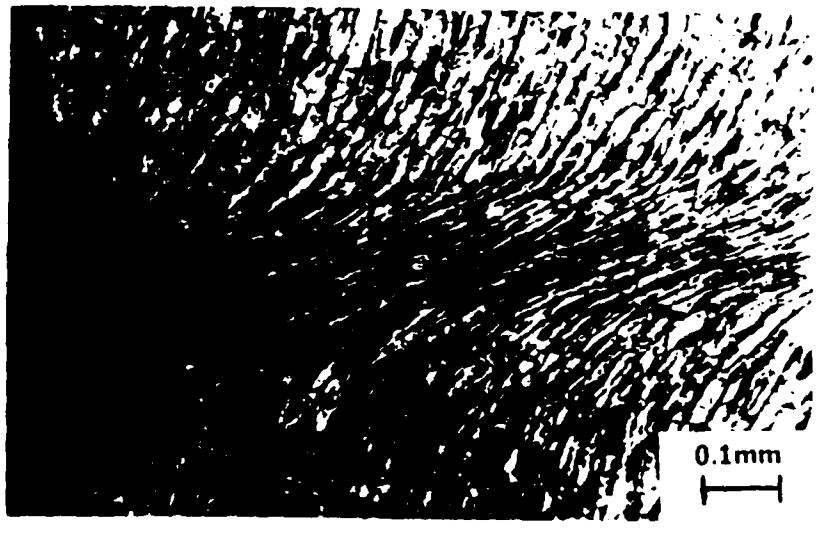

Figure 16: 1018 CRS Specimen Etched in Nital to Reveal Microstructure After Shear Localization (Specimen 164)

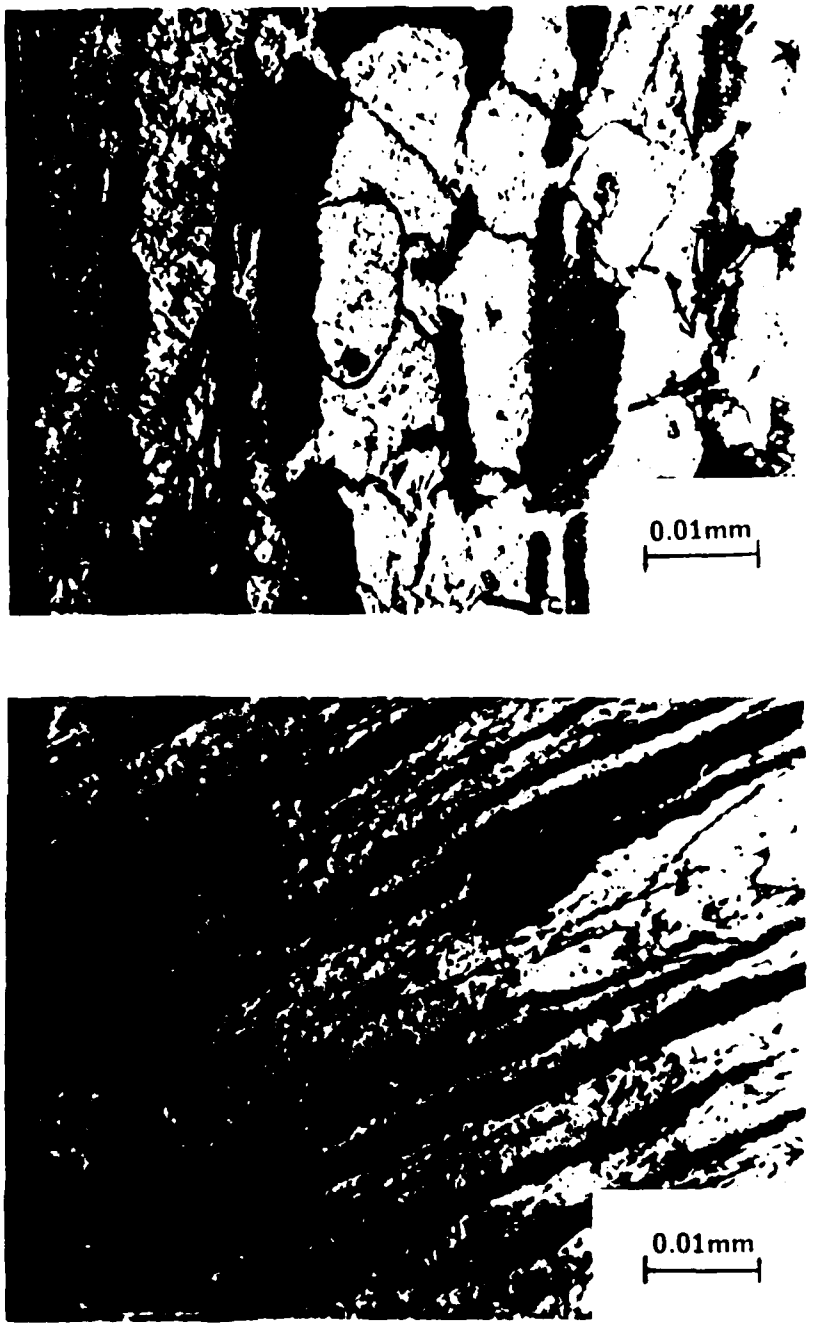

Figure 17: 1018 CRS Specimen Etched With Nital to Show Shear Band Microstructure (Specimen 164). Top Photograph Shows Undeformed Material, Bottom Photograph Shows Shear Band Material.

Temperature Measurement-250 Micron Spot Size

The first series of temperature measurements was performed focussing on ten spots each with a width of 250 microns (0.01 in.), approximately the same width as that of the shear bands that form in the CRS. Because the shear band may develop at any location across the gage length of the specimen (although, in steel, bands have never been seen to develop near the flanges) this spot size allowed measurements along the entire gage length and thus assured that at least one measurement would be taken in the shear band region. At this magnification, the separation between elements on the detector plane leads to a spatial gap between observed spots on the specimen of 0.08 mm (0.003 in). Figure 18 shows the output of two adjacent I-R detector elements during a test with Specimen 90, as well as the temperature profile across the gage section for the same test at the time of peak temperature. It can be seen that the maximum temperature of 206°C occurred near the center of the specimen, with the temperature dropping off rapidly to either side. It seems unlikely that in any of the tests the viewing area of one detector element covered only the shear band width and none of the cooler adjacent material. Hence, the detector output undoubtedly underestimates to some extent the average shear band temperature. The maximum shear band temperature recorded in any of the tests with the 250 micron spot size was 240°C. This value compares well with the temperature increase computed from the heat generated by the plastic work, as calculated in the following section.

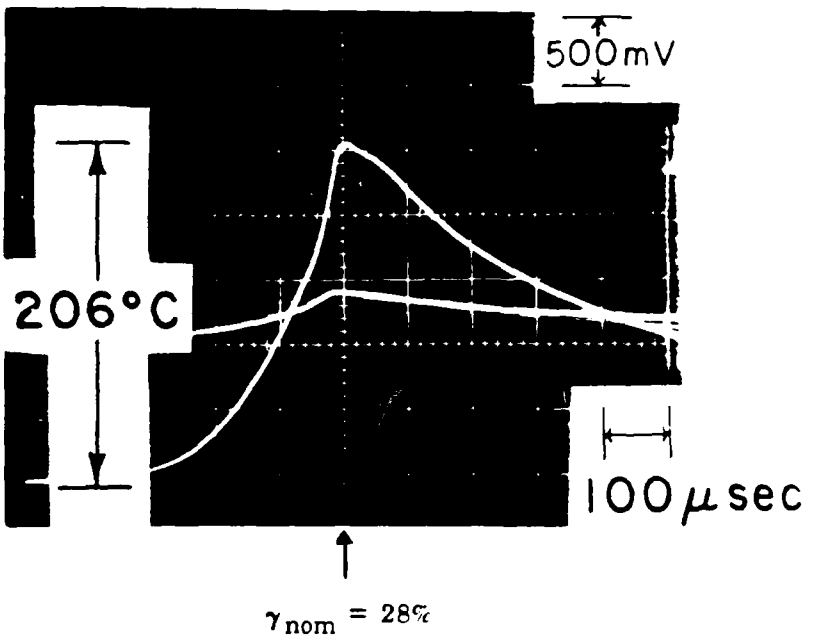

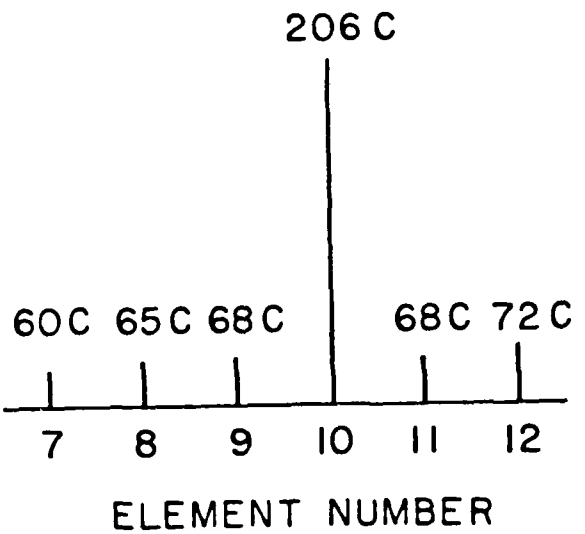

Figure 18: Output of Two I-R Detector Elements and Temperature Profile (1018 CRS, Specimen 90; 250 micron spot size)

Calculated Temperature Increase in the Shear Band Due to Plastic Work

The temperature measured across the shear band using the infrared detection system can be compared with an estimate of the heat generated by plastic work. For a plastic strain increment $d\gamma^p$, the increment of plastic work is given by:

$$dW^p = \tau \, d\gamma^p$$

Assuming that ninety percent of this work is transformed into heat, the increase in temperature at the band will be:

$$\Delta T = 0.9W^p / J\rho_o c$$

Here, $W^p = \int \tau d\gamma^p$ is the total plastic work at the shear band and hence is approximately equal to the area under the stress - strain curve, ρ_o = 7.8 gm/cm^3 and c = 0.118 cal/gm°C. In the experiment, the plastic work can be estimated by multiplying the total shear band strain by the measured stress averaged over the test duration. Because the shear stress can be considered identical at every cross section of the specimen (at least after the first few microseconds following the arrival of the pulse), the shear band stress is given by the output of the gages on the transmitter bar and can be determined reliably using oscilloscope records. In cold rolled steel, the strain hardening rate is low and the flow stress remains nearly constant throughout the test, Figure 19, and hence the stress can be approximated quite accurately by the stress level averaged over the test. The shear band strain, however, is much more difficult to determine, since the strain measured with the Kolsky bar is only an average for the entire specimen length. Furthermore, the instant when the shear band begins to form is not known precisely, nor is its width as it develops, so that Kolsky bar records provide only an estimate and not reliable

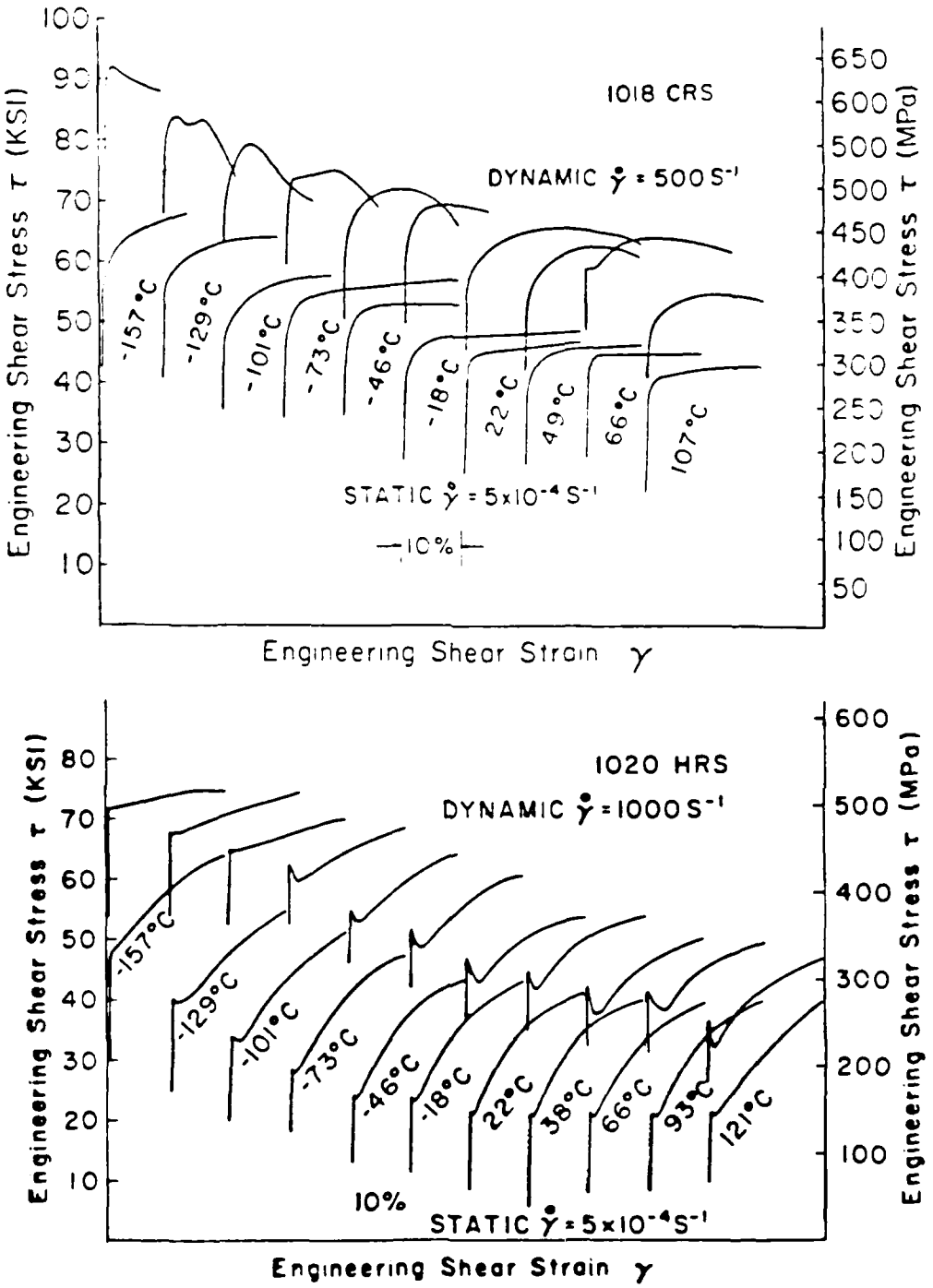

Figure 19: Shear Stress-Shear Strain Curves for 1018 CRS and 1020 HRS from Costin et al. [12]

values of shear band strain. Accordingly, the final strain in the shear band was estimated by measuring the inclination of the scribe lines after testing, taking into account the fact that the strain is not constant across the band. Using post-test photographs of the specimen, the average scribe line inclination was approximated by a straight line across the band, and this value was used to give the average shear band strain. For specimen 90, the average strain in the band was 260 percent, leading to a calculated temperature increase of 220°C. This simple calculation gives a temperature for the band that is very close to that measured with the infrared system using a spot width on the order of the width of the band. However, because the final strains in the central portion of the band are much higher than the average band strain used, it seems likely that the temperature near the center of the band was considerably higher.

Temperature Measurement-20 Micron Spot Size

In order to examine the temperature profile within the shear band, the optical arrangement was adjusted so each of the ten detector elements was focussed on a 20 micron spot size on the specimen. Since the shear bands in the CRS are about 250 microns wide, this spot size can provide a good measure of the temperature profile across the band. However, the entire array of ten detectors covers a width of only 260 microns, so that some of the tests were unsuccessful because the shear band formed to one side of the viewing area. In no test did the shear band occur directly in the center of the array of elements. However, a number of tests were successful. For instance, in specimen 165 the maximum output was recorded by element 9 as 54 mv which corresponds to a rise of 420°C. The temperature variation in this test, shown in Figure 20, demonstrates that a large temperature gradient develops across the shear band in CRS. This result is consistent with the highly inhomogeneous strain profile evident from the scribe lines after testing. The output

of the detector element showing the largest increase (element 9) is converted to the temperature scale using the calibration curve of Figure 11. In Figure 21, temperature is plotted as a function of time along with the simultaneous stress-time record from the output of the gages on the transmitter Kolsky bar. Temperatures less than about 80°C cannot be determined since the noise to signal ratio in the I-R signal becomes too great. However, the maximum recorded temperature rise in this test is about 420°C, significantly higher than the average temperature of 240°C measured with the 250 micron spot size. Thus, the maximum temperatures within the band are considerably higher than the average.

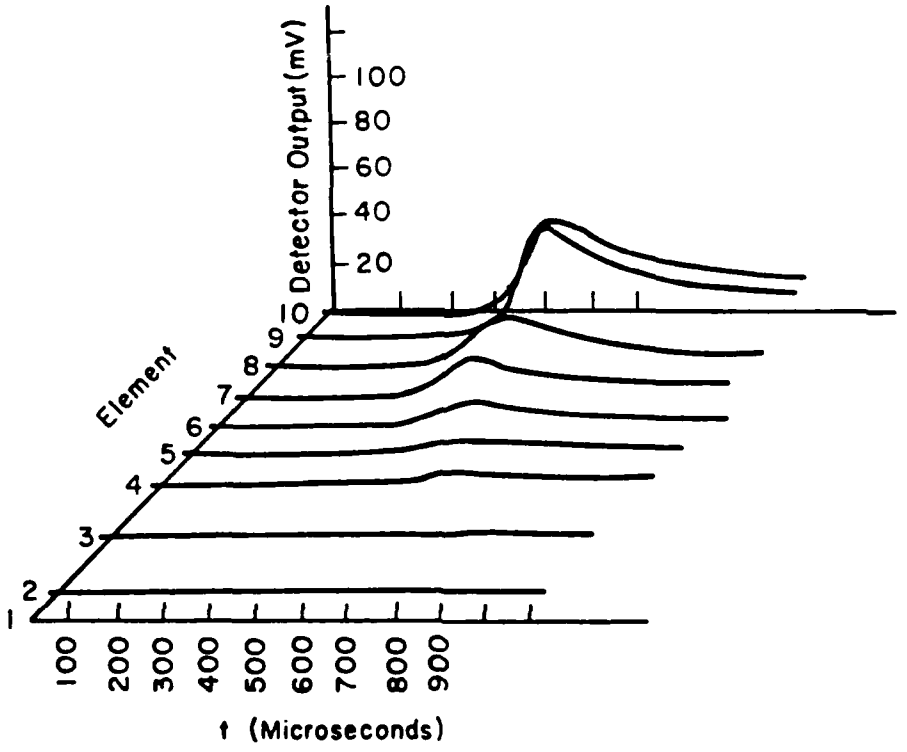

Figure. 20: Spatial Profile of I-R Detector Output (20 Micron Spot) During Shear Band Formation in 1018 CRS; Specimen 165. The maximum detector output is for element 9, corresponding to a maximum temperature rise of 420°C.

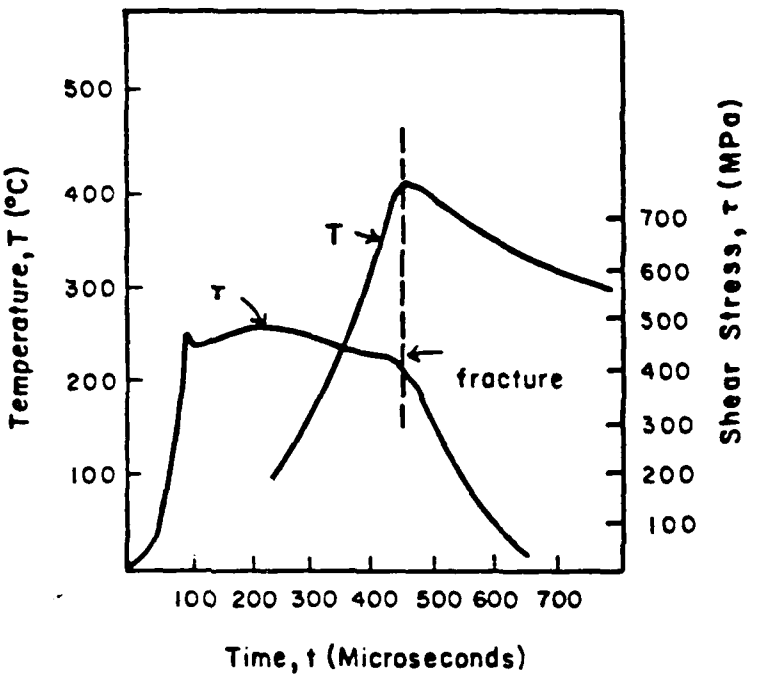

Figure 21: Shear Band Temperature and Stress As Functions of Time (20 Micron Spot, Specimen 165) in 1018 CRS

Comparison With the Analysis of Shawki and Clifton

In order to examine the effects of strain hardening, of thermal softening and of strain rate sensitivity on shear band formation in both cold rolled and hot rolled steels, a complete numerical analysis was performed by Shawki et al. [16] and by Clifton et al. [17]. The analysis was carried out for simple shear, allowing for easy comparison with the behavior observed in the present experiments. In the analysis, an initial geometric imperfection was utilized as a shear band nucleator, Figure 22, playing the role of a circumferential machining defect in the actual specimens. The study included the effects of both inertia and heat conduction, and made no assumption of deformation homogeneity either within or outside the shear band. The governing equations for this problem can be written as:

- Momentum Balance: $\rho_0 v_t = \tau_y$
- Compatibility: $\gamma^p{}_t = v_y$
- Energy Balance: $\rho_0 T_t = kT_{yy} + \beta\tau\gamma^p{}_t$
- Constitutive Equation: $\tau = \tau(\gamma^p, \dot{\gamma}^p, T)$

where v is the particle velocity, T the temperature, τ the shear stress, and γ^p the plastic shear strain. The parameters ρ_0, c, k, and β are, respectively, the mass density, the specific heat, the thermal conductivity and the portion of the plastic work converted to heat. Subscripts y and t denote partial differentiation with respect to the axial dimension and to time, respectively, and the primary variables are taken as functions only of y and t. The full solution of the nonlinear system of equations for simple shear was determined by Shawki [28] using a finite difference scheme.

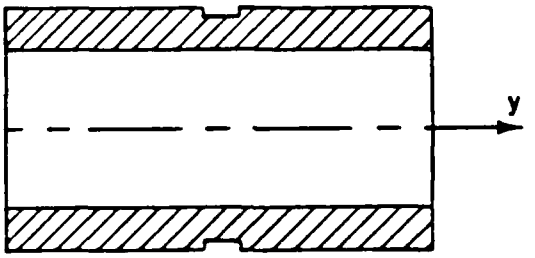

Figure 22: Specimen Geometry. (ref. Shawki et al. [16])

To model the behavior of the two steels, a power-law constitutive equation of the form:

$$\tau = \tau_0 T^{\nu}(\dot{\gamma}^p)^m(\gamma^p)^n$$

was used. The material parameters τ_0, ν, m and n were evaluated from a least squares fit of the experimental results of Costin et al. [12], given in Figure 19, supplemented by present test results. The resulting values are presented in Table 3. For all the numerical calculations the imposed dynamic strain rate was taken as $10^3 s^{-1}$.

Table 3: Table of Material Parameters Used in Analytical Model (ref. Shawki et al. [16])

	1018 Cold Rolled Steel	1020 Hot Rolled Steel
ν	-0.38	-0.51
n	+0.015	+0.12
m	+0.019	+0.0133
τ_0	436 MPa	261 MPa
k	54 W/m^{o}C	
ρ_0	7.8 gm/cm^3	
c	500 J/kg^{o}C	

Figure 23 shows some of the results of Shawki et al [16] for the cold rolled steel. There is a dramatic growth in strain, in strain rate and in temperature within the shear band relative to the material outside the band. At a nominal strain of twenty percent, both the strain and temperature are highly localized and all further strain is concentrated within the shear band in the center of the groove. To determine the critical strain for shear band formation, Clifton et al. [17] employed a norm ratio of the strains. This norm ratio provides a measure of the strain within the shear band compared with the strain in the material outside the band. Its values for the CRS are plotted in Figure 24. It can be seen from this figure that the predicted shear band strain increases as nominal strain increases and becomes infinite at a nominal plastic strain of about 23 percent. The calculations also show that the flow stress reaches a maximum across the specimen at approximately twelve percent strain. This agrees well with the experimental results from the stress-strain curve. In Figure 25 the temperature profile for CRS previously shown in Figure 23 is replotted and compared with experimental results obtained for specimen 90 using the infrared

radiation detection system. As may be seen, for the point for which a comparison is possible there is good quantitative agreement between the results of the experiments and analysis. For other locations on the specimen's surface the experiment indicates only that the temperature rise is less than about 80°C. This indicates that with the geometric imperfection method of shear band nucleation used in the numerical scheme it is possible to predict quite accurately shear localization behavior in this steel based solely on constitutive parameters derived from experiments.

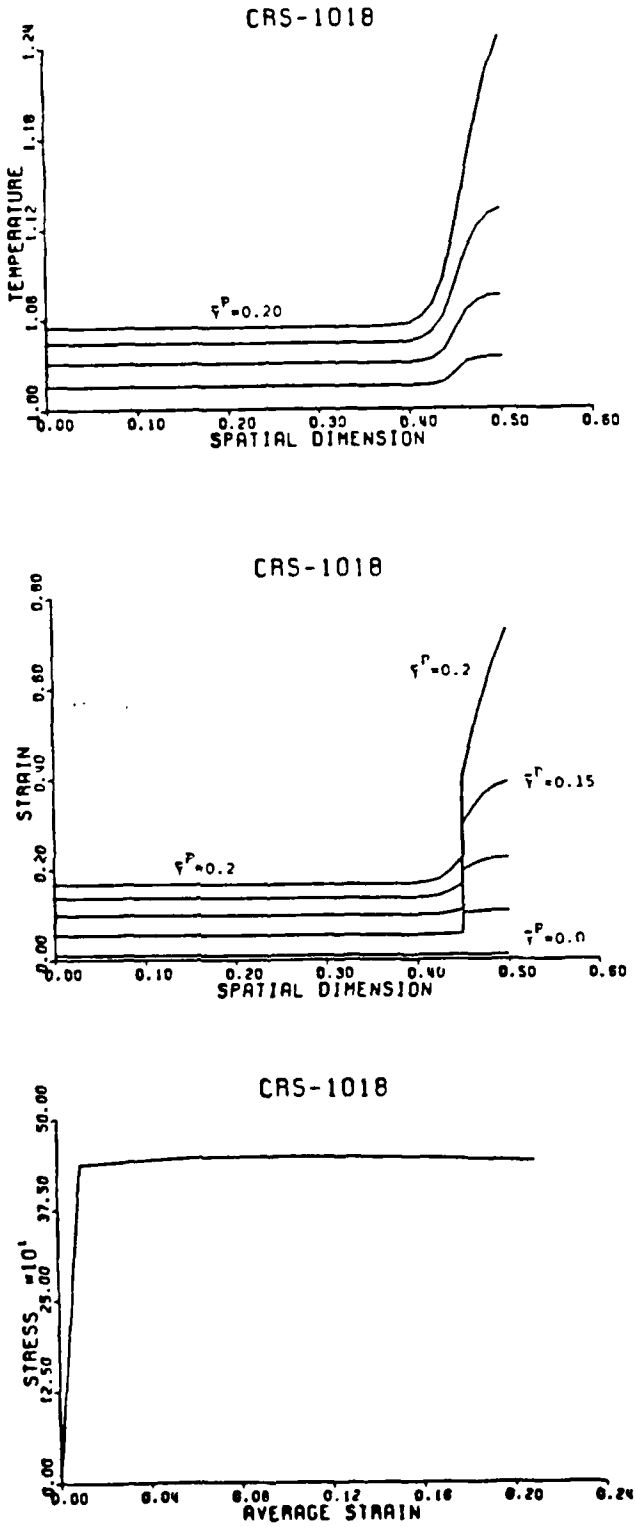

Figure 23: Results of Numerical Model for 1018 CRS. (ref. Shawki et al. [16])

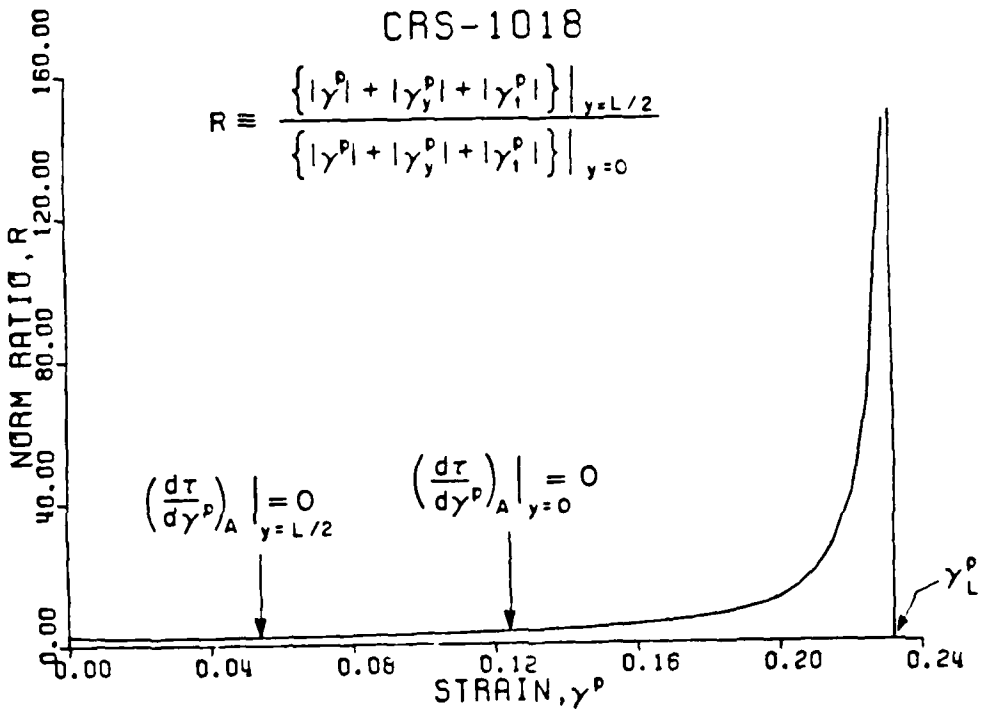

Figure 24: Norm Strain Ratio Showing Localization in CRS. (ref. Shawki et al. [16])

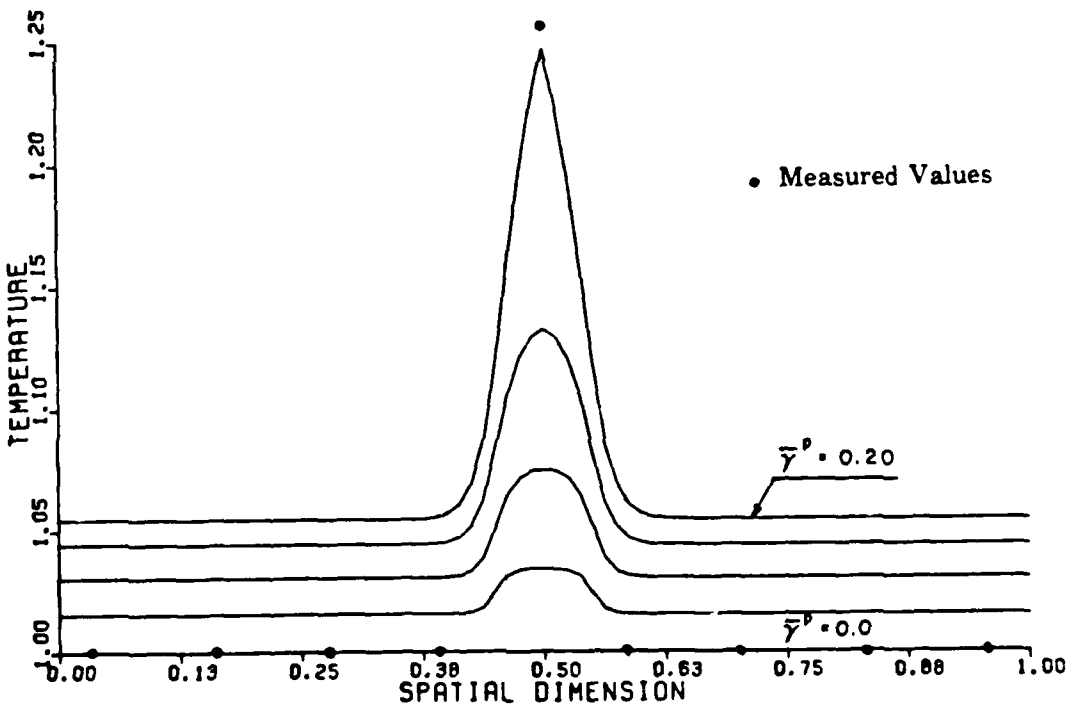

Figure 25: The Temperature Profile for 1018 CRS Calculated by Clifton and Shawki (Solid Lines) Compared With Measured Values of Temperature (Specimen 90)

RESULTS OF TESTS WITH AISI 1020 HOT ROLLED STEEL

In this section, results are presented showing that shear bands do develop in AISI 1020 hot rolled steel (HRS) when the imposed dynamic strains are sufficiently great. In addition to the experimental results, the analytical study by Shawki, et al. [16] and by Clifton, et al. [17] is applied to these steels and shows good agreement with the observed behavior of the HRS.

Costin, et al. [12] performed a series of tests on specimens of a CRS and of a HRS and found that a shear band developed in each test with the CRS but that none forms in the HRS when deformation is limited to about thirty percent. The two steels have similar chemistries, and tests at two different strain rates and over a broad spectrum of temperatures showed that the two steels have very similar strain rate sensitivities and thermal softening rates. The strain hardening effect, however, is almost an order of magnitude higher in the HRS, and it was thought that this difference combined perhaps with the lower flow stress at low strains, was responsible for inhibiting shear band formation in the HRS. Accordingly, Costin et al. prestrained a specimen of a HRS quasi-statically in the Kolsky bar until both the level of stress and the strain hardening rate were about equal to those of the CRS. After this prestraining, the specimen was tested dynamically in the torsional Kolsky bar. While a shear band had been expected, the deformation turned out to be homogeneous. The reason remains unclear but the effect of material texture on shear band behavior is still not well understood, and may play a role in this apparent anomaly.

In addition to their experimental work, Costin et al. performed an analysis of the behavior of the HRS based on a model proposed by Litonski [30]. The results were consistent with those of the experiments: at a nominal strain of thirty percent

there was very little difference in strain or temperature between the material inside or outside the initial groove. A similar analysis for the CRS showed a considerable difference in both strain and temperature indicating shear band development at about thirty percent nominal strain. Semiatin [31] carried the calculations with Litonski's model to higher values of nominal strain, and found that HRS would eventually show strain localization within the groove. This same result was predicted by Shawki and Clifton [16], using the model previously described that does not require homogeneity of strain, strain rate or temperature either inside or outside the band. Shawki and Clifton predicted the formation of shear bands in HRS at nominal strains of 80 to 100 percent, and later experiments confirmed their existence at about these strains.

Mechanical Behavior

In view of the predictions of the analysis, it was decided to test 1020 HRS to larger values of strain. The composition of the steel is given in Table 4 and a list of the tests performed in Table 5, in which the symbols have the same meaning as in Table 2. The larger imposed values of strain were achieved by increasing the strain rate to the range 2000 s^{-1} to 5000 s^{-1} while preserving the same pulse length. A typical shear stress-shear strain curve is shown in Figure 26, and a comparison of results, Tables 2 and 5, shows that a maximum flow stress does occur in HRS but, indeed, requires considerably more strain than needed in CRS.

Table 4 1020 HRS: Chemical Composition (Weight Percent)

C	Mn	P	S
0.26	0.50	0.018	0.030

TABLE 5: List of Tests Performed with 1020 HRS

Spec. No.	$\dot{\gamma}$ sec^{-1}	γ_{max} %	τ_y MPa	τ_{max} MPa	γ at τ_{max} %	Shear Band Fracture	Spot size (microns)	Max ΔT(°C)
317	2200	102	296	386	80		20	
320	4600	180	290	393	140	SB, F	20	
324	2300	80	296	379	68	SB, F[1]	20	455
325	2000	80	290	382	70		20	
326	2200	65	296	372	55	SB, F[1]	20	370
327	2800	124	290	386	80	SB, F	20	
329	2400	100	296	396	75	SB	20	150
330	2200	100	296	390	70	F[1]	20	
331	4800	130	283	390	110	SB, F	20	
332	5100	170	282	390	130	SB, F	20	
333	3200	144	303	414	110	SB, F	20	
341	2400	92	350	410	40	SB, F	250	175
342	3000	134	283	400	90	SB, F	250	240
343	2600	67	296	386	65	SB, F[1]	20	

After each test, the specimen was examined and it was found from the scribe lines that a shear band did indeed form in HRS but only when higher values of nominal strain are imposed. The presence of a shear band is also apparent from the temperature measurements, which will be discussed in the following sections. An example of a shear band in this steel, one containing a fracture, is shown in Figure 27. In general, shear bands in the HRS are narrower than those in CRS; about 150 microns (0.003 inches) wide, as compared with 250 microns (0.005 in) in the CRS. As in CRS, whenever a specimen fractures, the crack appears approximately along the center line of the shear band.

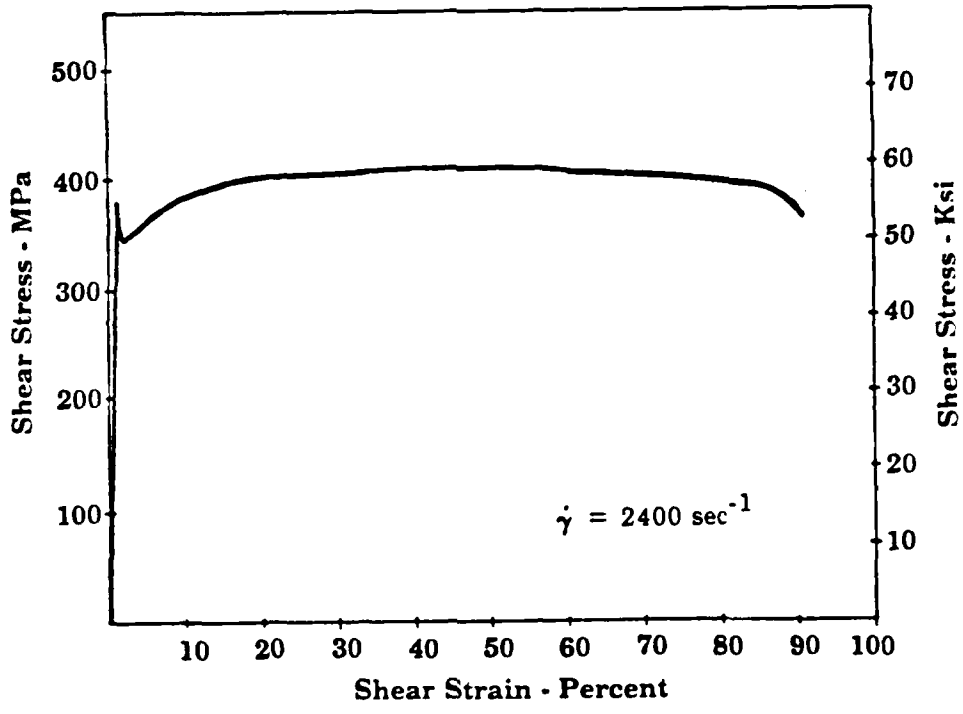

Figure 26: Shear Stress - Shear Strain Curve for 1020 HRS (Specimen No. 341)

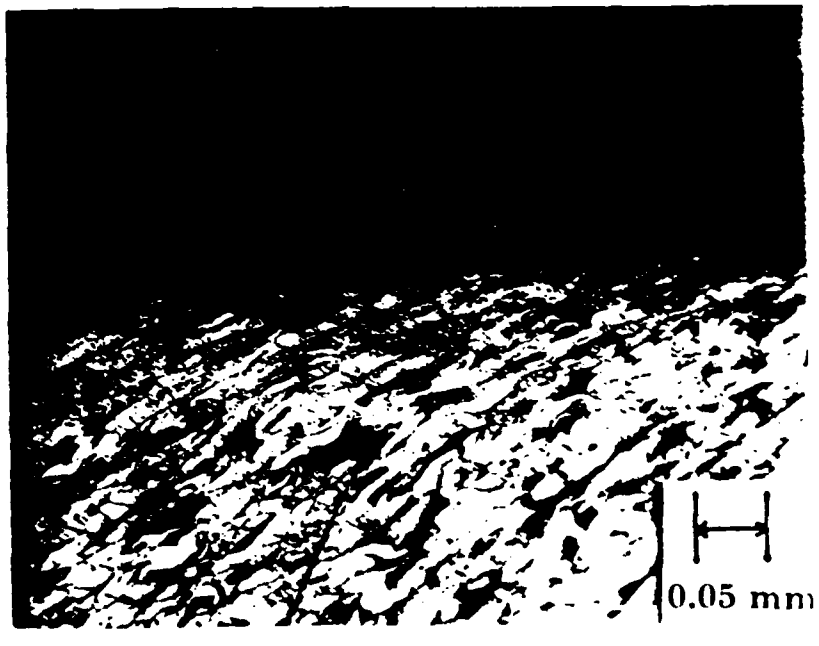

Figure 27 Shear Band in 1020 HRS, Etched in Nital to Reveal Microstructure. The Specimen Fractured During Deformation and Only One Half of it is Shown in the Photograph. (Specimen 324)

Temperature Measurement - 250 Micron Spot Size

With each of the detector elements focussed on a 250 micron spot size, the the array of detectors covered the entire gage section and provided results that could be compared easily with the results of the tests on CRS. At this magnification the spatial gap on the specimen between observed spots is about 75 microns (0.003 in). and since the shear bands themselves are about 150 microns wide the observed area must have included some of the colder material to either side of the shear band. Hence, the actual shear band temperature must be somewhat higher than the temperature measured by this method. In many of the tests it was found that an inhomogeneous temperature profile did develop across the specimen. Thus the temperature measurements, as well as observations of the scribe lines after testing, indicate that shear bands will form in the HRS, although they develop only at much higher values of nominal strain than in the CRS.

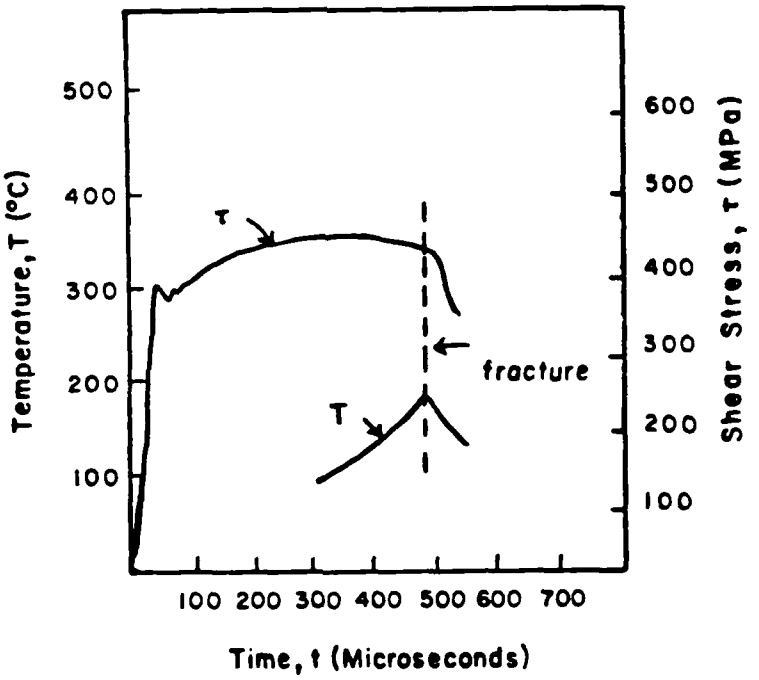

Figure 28: Stress and Shear Band Temperature as Functions of Time for HRS. (250 micron Spot, Specimen 341)

Figure 28 shows the shear stress in the specimen as a function of time for HRS deforming dynamically. The output of the IR detector indicating the maximum temperature during the same test is also shown in the figure on the same time scale. Since the noise to signal ratio is large at lower temperature, no output is shown for the first 300 microseconds. From then on the temperature increases to a rather sharp peak, which is presumed to represent fracture, since the maximum in temperature also coincides with a sharp and rather large drop in the recorded value of stress. The highest temperature measured for specimen 341 is about 175°C, but there was a considerable variation in the highest temperature for different specimens with a maximum 240°C for Specimen 342. In order to measure the higher temperatures that are expected at the center of the bands in the HRS, further tests were conducted using a higher magnification.

Temperature Measurement - 20 Micron Spot Size

As explained previously, the temperature can be measured over a spot 20 microns wide by adjusting the optical system appropriately. The smaller spot width allowed for detailed measurements over the entire shear band width. However, when the total width observed on the specimen by the entire array of 10 detector elements measures only 260 microns, then it is quite likely that the shear band will form outside the observed area. Accordingly, some specimens were prepared with a shallow circumferential groove that triggered shear band nucleation in a designated area. These tests are marked "1" in Table 5. Figure 29 shows the detector output from a test with a 20 micron spot width. As is evident from the figure, there is an irregularity in the output signal of about 50 microseconds duration that occurs shortly after the peak output. The most likely explantion for this irregularity is that it is associated with the presence of the groove, since it was not seen in tests with other steels where no groove was present.

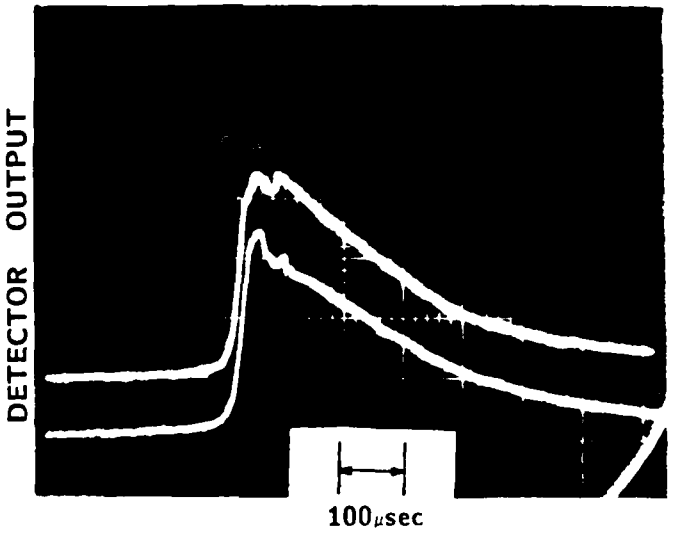

Figure 29: Output of Two Detector Elements (HRS Specimen 324, 20 Micron Spot)

The maximum shear band temperature measured with the 20 micron spot size was 455°C in specimen 324. This is slightly higher than the temperature measured in the shear bands in the CRS with the same magnification. The band temperature is significantly higher than the average shear band temperature measured with the 250 micron spot width. This is consistent with the presence of a strain gradient across the band, which provides appreciably more plastic deformation near the band center. Figure 30 gives the temperature profile across a shear band and shows that the temperature increases gradually across the band. The array of detectors happened to be so located that the maximum temperature was reached at the outermost detectors. In the following section, this measured temperature profile is compared to the results of an analytical model for shear banding.

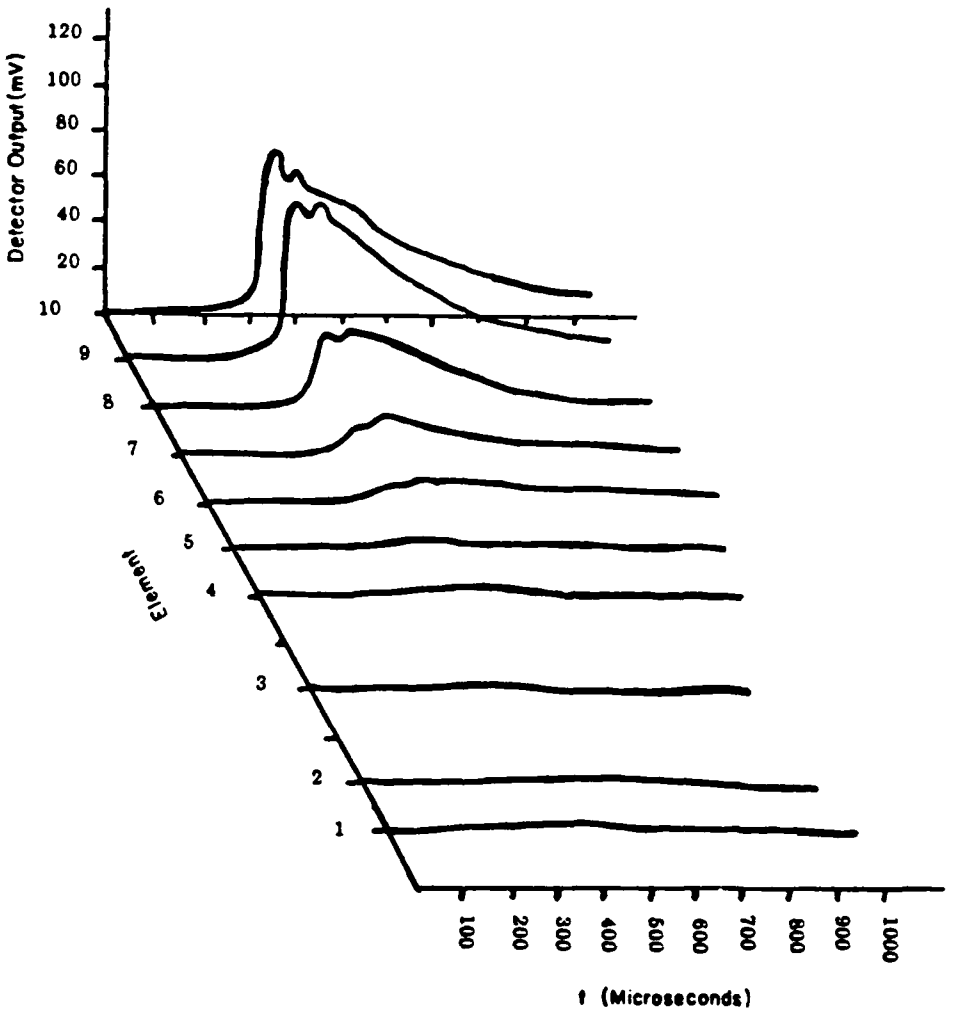

Figure 30: Spatial Profile of I-R Detector Output (HRS Specimen 324, 20 Micron Spot)

Comparison With the Analytical Results of Shawki and Clifton

Shawki applied the model previously described, to study the deformation of the 1020 HRS [16, 17]. As before, the material parameters used in the constitutive relation were derived from the present experiments and those of Costin et al. [12]. These parameters are presented in Table 3, from which it can be seen that the most important difference between the two steels is the value of n, the strain hardening parameter, which is almost an order of magnitude larger in the HRS. Thus the rate of strain hardening probably plays an important role in the tendency toward strain localization. According to the analysis, some difference in strain and in temperature is expected between the material inside and outside the groove used in the model, but even at a nominal strain of thirty percent the difference is not pronounced. This is consistent with the observation of Costin et al. that no shear bands developed in the HRS at thirty percent strain. Furthermore, under the same conditions the predicted behavior of HRS differs considerably from that of CRS (Figure 23). At a strain rate of $10^3 s^{-1}$, the strain in the CRS always becomes highly localized by a nominal strain of 20 percent, with nearly all further strain concentrated within the shear band. This is probably due to the low strain hardening rate of the CRS, which allows the thermal softening in the band to dominate. To determine if localization occurs in HRS at a high enough value of nominal strain, Shawki [28] extended the analytical solution described above to high strains. In Figure 31, the norm strain ratio is plotted as a function of nominal strain. It can be seen that the strain eventually becomes localized within the groove at a nominal strain of about ninety percent. This prediction agrees well with the present experimental results, which show that localization does indeed occur in the HRS at strains of about 80 to 100 percent. Overall, one may conclude that the computations based on the homogeneous properties of the material in both the CRS and the HRS appear to model the experimental

observations quite accurately, in spite of a very different behavior with respect to shear bands: one steel showing considerably more tendency toward strain localization than the other.

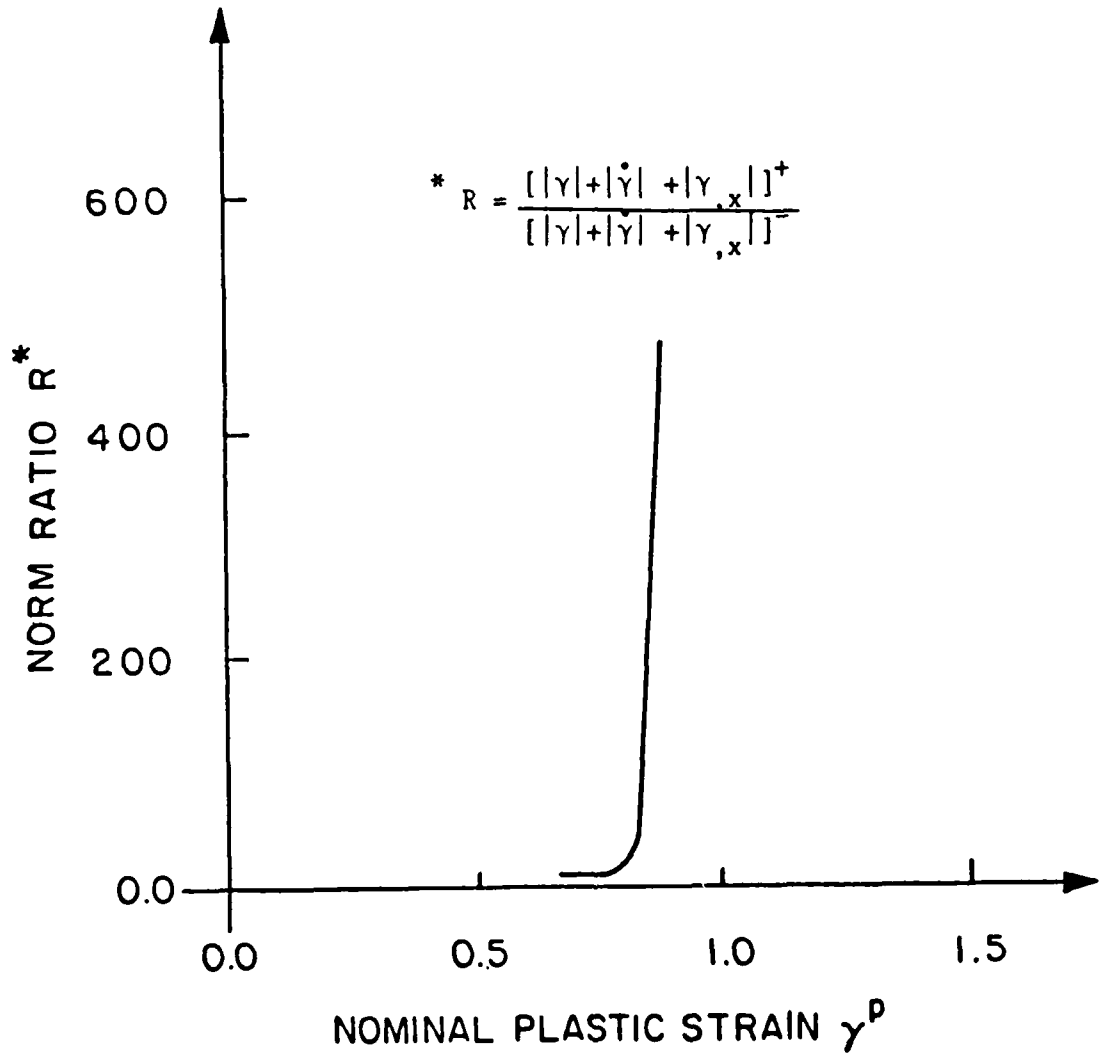

Figure 31: Norm Strain Ratio Showing Localization in HRS. (Shawki [28])

CONCLUSIONS

A series of experiments was performed to study the formation of shear bands in steel, including measurements of the temperature profile across the shear band during its formation. These temperature measurements were effected by monitoring the infrared radiation emitted from the surface of the specimen during dynamic deformation in a torsional Kolsky bar. Two low carbon steels were tested at strain rates in the range 1000 to 5000 sec^{-1}. Shear bands occurred in both steels and are relatively wide, about 250 microns in 1018 cold rolled steel (CRS) and 200 microns in 1020 hot rolled steel (HRS). These bands did not etch white in nital and the strain in the bands increased gradually from the uniform strain outside to a maximum in the center of the band.

A linear array of ten indium-antimonide detectors was employed to measure the infrared radiation from the developing shear bands. A spherical mirror was used to focus the radiation onto the detectors, and the distance of the mirror from the specimen and from the detectors was used to fix the diameter of the observed spot on the surface of the specimen. Two spot sizes were utilized for these tests: one with a diameter of about 250 microns, and one of about 20 microns. The latter spot size enabled us to determine the temperature profile across the shear bands in the two steels. It was found that shear bands are accompanied by large temperature gradients and that these gradients continue to grow with further deformation, often until fracture. Temperature increases as high as 450°C occur at the band center as measured with the 20 micron spot width. The temperature is found to vary considerably across the width of the band, as is suggested also by the inhomogeneous permanent strain profile indicated by the scribe lines after testing. An analytical model by Shawki and Clifton using parameters derived from the stress strain curves for the two steels predicts accurately both the temperature profile across the gage section for the CRS and the critical strain for shear localization in each

of the steels. This is true despite their different strain hardening behavior, and despite the fact that shear bands in the CRS form at about 10 or 15 percent strain while about 100 percent strain is needed for localization in the HRS.

ACKNOWLEDGEMENTS

The research support of the Army Research Office under Grant DAAG29-85-K-003 and the NSF Materials Research Laboratory at Brown University are gratefully acknowledged. The technical assistance of G.J. LaBonte, Jr. is also appreciated.

REFERENCES

1. Rogers, H. C., "Adiabatic Shearing - A Review," Drexel University Report, U. S. Army Research Office, 1974.

2. Rogers, H. C., "Adiabatic Plastic Deformation," *Annual Reviews in Materials Science*. Vol. 9, p. 283, 1979.

3. Hutchinson, J.W., "Viewpoint Set on Shear Bands" Scripta Metallurgica, Vol. 18, No. 5, May, 1984.

4. Olson, G., Mescall, J. F. and Azrin, M., "Adiabatic Deformation and Strain Localization," *Proc. Conf. on Shock Waves and High Strain Rate Phenomena*, M. A. Meyers and L. E. Murr, Eds., Plenum Press, New York, p. 221, 1981.

5. Clifton, R. J., "Adiabatic Shear Banding," Chapter 8, *Material Response to Ultra High Loading Rates*, National Materials Advisory Board Committee, Rep. No. NMAB-356, 1980.

6. Bedford, A. J., Wingrove, A. L. and Thompson, K. R. L., "The Phenomenon of Adiabatic Shear Deformation," J. Aust. Inst. Metals, Vol. 19, p. 61, 1974.

7. Basinski, Z. S., "The Instability of Plastic Flow of Metals at Very Low Temperatures II," Australian Phys., Vol. 13, p. 354, 1960.

8. Recht, R. F., "Catastrophic Thermoplastic Shear," J. Appl. Mech., p. 189, 1964.

9. Argon, A. S., "Stability of Plastic Deformation," *The Inhomogeneity of Plastic Deformation*, American Society for Metals, 1973.

10. Culver, R. S., "Thermal Instability Strain in Plastic Deformation," *Metallurgical Effects at High Strain Rates*, R. W. Rohde, B. M. Butcher, J. R. Holland and C. H. Karnes, Eds., Plenum Press, N. Y., p. 519, 1973.

11. Staker, M. R., "The Relation Between Adiabatic Shear Instability Strain and Materials Properties," Acta Metall., Vol. 29, p. 683, 1981.

12. Costin, L.S., Crisman, E.E., Hawley, R.H. and Duffy, J., "On the Localization of Plastic Flow in Mild Steel Tubes Under Dynamic Torsional Loading," *Proc. of the 2nd Conference on the Mechanical Properties of Materials at High Rates of Strain*, J. Harding, Ed., The Institute of Physics, London, p. 90, 1979.

13. Merzer, A. M., "Modelling of Adiabatic Shear Band Development from Small Imperfections," J. Mech. Phys. Solids, Vol. 30, No. 5, p. 323, 1982.

14. Bai, Y. L., "Thermo-Mechanical Instability in Simple Shear," J. Mech. Phys. Solids, p. 195, 1982.

15. Fressengeas, C. and Molinari, A. "Inertia and Thermal Effects on the Localization of Plastic Flow," Acta. Metall., Vol. 33, p. 387, 1985.

16. Shawki, T., Clifton, R. J. and Majda, G., "Analysis of Shear Strain Localization in Thermal Visco-Plastic Materials," Brown University Report No. ARO DAAG29-81-K-0121/3, 1983.

17. Clifton, R. J., Duffy, J., Hartley, K. A. and Shwaki, T. J., "On Critical Conditions for Shear Band Formation at High Strain Rates," Scripta Met., Vol. 18, p. 443, 1984.

(?) Jonas, J. J., Holt, R. A. and Coleman, C. E., "Plastic Stability in Tension and Compression," Acta Met., Vol. 24, p. 911, 1976.

18. Wu, F.W., Toulios, M. and Freund, L.B., "Initiation and Propagation of Shear Bands in Antiplane Shear Deformation," Brown University Report No. DAAG-29-81-K-0121, 1984.

19. Kolsky, H., "An Investigation of the Mechanical Properties of Materials at Very High Rates of Loading," Proc. Phys. Soc., London, V62-B, p. 676, 1974.

20. Baker, W. W. and Yew, C. H.,, "Strain Rate Effects in the Propagation of Torsional Plastic Waves," J. Appl. Mech., Vol. 33, p. 917, 1966.

21. Nicholas, T., "Strain-Rate and Strain-Rate History Effects in Several Metals in Torsion," Exp. Mech., Vol. 11, No. 8, p. 370, 1971.

22. Duffy, J., Campbell, J. D. and Hawley, R. H., "On the Use of a Torsional
Split-Hopkinson Bar to Study Rate Effects in 1100-O Aluminum," J. Appl. Mech., Vol. 38, p. 83, 1971.

23. Lindholm, U.S. "Some Experiments with the Split-Hopkinson Pressure Bar," J. Mech. Phys. Solids, Vol. 12, No. 5, p. 317, 1964.

24. Hartley, K. A., Duffy, J. and Hawley, R. H., "The Torsional Kolsky (split-Hopkinson) Bar," *Metals Handbook*, Vol. 8, American Society for Metals, p. 2168, 1985.

25. Hayashi, T., Yamamura, H. and Okano, S., "Temperature Measurement of Metals Under High Velocity Deformation," *Twentieth Japan Congress on Materials Research*, Society of Materials Science, Kyoto, Japan, p. 94, 1977.

26. Moss, G. L. and Pond, R. B., "Inhomogeneous Thermal Changes in Copper During Plastic Elongation," Met. Trans., Vol. 6A, p. 1223, 1975.

27. Duffy, J. "Temperature Measurements During the Formation of Shear Bands in a Structural Steel," Mechanics of Material Behavior, The Daniel C. Drucker Anniversary Volume, G.J. Dvorak and R.T. Shield, Eds., Elsevier, p. 75, 1984.

28. Shawki, T. J., "Analysis of Shear Band Formation at High Strain Rates and the Visco-Plastic Response of Polycrystals," Ph. D., Thesis, Brown University, 1985.

29. Costin, L. S., Server, W. L. and Duffy, J., "Dynamic Fracture Initiation: A Comparison of Two Experimental Methods," J. of Engr. Materials and Technology, Vol. 101, p. 168, 1979.

30. Litonski, J., "Plastic Flow of a Tube Under Adiabatic Torsion," *Bulletin de l'Academie Polonaise des Sciences*, Vol. 25, p. 7, 1977.

31. Semiatin, S. L., Private Communication.